NTNU – Trondheim
Norwegian University of
Science and Technology

Shallow gas AVO analysis in Block 2/4 North Sea

Chunlei Wang

Petroleum Geosciences
Submission date: June 2014
Supervisor: Martin Landrø, IPT
Co-supervisor: Per Avseth, IPT

Norwegian University of Science and Technology
Department of Petroleum Engineering and Applied Geophysics

Norwegian University of Science and Technology

Department of Petroleum Engineering and Applied Geophysics

Shallow gas AVO Analysis in Block 2/4 North Sea

Author:

Chunlei Wang

Supervisor:

Pr. Martin Landrø

Acknowledgement

First of all, I would like to express my sincere thanks to International Master Program in NTNU for giving me a great opportunity to come to Trondheim and study advanced knowledge and technology in Norway. The two years study period left such an impressive and indelible mark on my whole life.

My Master thesis has been done under the supervision of Professor Martin Landrø (NTNU). I would like to express my sincere gratitude to my supervisor professor for his advice and assistance during the development of this thesis. I admire his professional knowledge and appreciate his guidance and supportive through every step of this thesis. I would like to thank professors in the Petroleum Engineering and Applied Geophysics department, especially to Professor Egil Tjåland, Per Avesth and Ståle Emil Johansen. I appreciate their encouraging and helping me during my study in our department.

Special thanks to all the people that have made my stay in Norway exciting and unforgettable. Two years study aboard experiences for me is precious and valuable. Thanks to all the international classmates for their warm companion like a whole family. Juan Carlos Gloria Lopez, Dicky Harishidayat, Togi Yonathan Sitinjak, Paola Rodríguez Masiu, Dulce Carolina Cruz, Gabriela Labastidas, Nikita Krivenko, Alexey Svyatkovskiy, Valentin Zuchuat, all the geo-family made these two years impressive and tried to motivate when we worked hard in the geo-cave basement. Special thanks to Juan Carlos Gloria Lopez and Kjersti Eidissen's helping and supporting in the thesis processing.

I would like to thank my beloved parents Lizhen Sun and Cai Wang for their unconditional love and support all this time. All the encouraging words during times when I study in this world-class university. I love you so much!!

Tusen Takk!

Abstract

The study site block 2/4 blowout area is challenging because of shallow thin sand and limitation of available well data. The high amplitude anomaly with fingering shape pattern was discovered at 520ms. This shallower sand layer is significantly thinner, but shows up clearly on the seismic data. This thesis aims to distinguish observed high amplitude anomaly affected by tuning effects from gas saturation and to estimate sand thickness and extension related to the blowout. The AVO cross-plot created from estimation of intercept and gradient showed the best deviation from the background trend out of the quadrant III, and the anomaly could be classified as a class III AVO anomaly. The capability of interpreting a reservoir is highly dependent of seismic resolution. The limitation of interpreting a high amplitude anomaly sometimes fails to yield a unique solution of hydrocarbon filled. Tuning effect as another main factor is prone to produce constructive interference. The optimization wedge model was applied successfully to conduct tuning thickness survey in an attempt to estimate the thickness of thin gas sand. The relationship of amplitude and tuning thickness between the near and far stack suggests that not only is the observed high amplitude anomaly affected by gas saturation, but also by tuning effect. The P-impedance data in seismic inversion model enhance the interpretability of high amplitude anomaly associated with tuning effects.

Contents

List of Figures

List of Tables

1 Introduction

The Amplitude-Versus-Offset (AVO) analysis is a commonly utilized effective technique for hydrocarbon detection, fluid content prediction and lithology identification. This technique has been successfully applied for hydrocarbon exploration quantitatively in North Sea reservoirs. During prospect drilling on the Norwegian Continental Shelf, shallow gas accumulations result in blowout that is hard to control due to the high pore pressure. This potential geohazard arises the interest to analyze the properties of this shallow gas sands in order to avoid or control them during drilling.

The study area for this thesis covers around $240km^2$ in block 2/4 in the southern part of North Sea, within the Nordland Group of Upper Pliocene age. In January 1989 Saga Petroleum experienced an subsurface blowout when drilling deep exploration well 2/4-14. There are clear indications from the variation of amplitude monitoring in 4D seismic data of where gas has migrated into shallower sand layers (above 1000ms). The monitoring of high amplitude anomaly around 520ms demonstrates the horizontal extent increases within almost twenty years. RMS amplitude extraction map illustrates some fingering-shape on the southeastern blowout area. Since the amplitude anomaly gradually weakens with distance from the blowout well, which illustrates that the gas saturation decreases away from the well, a precise estimate of the gas anomaly extension and sand thickness are difficult. The objective of this thesis is to estimate the thickness and extension of the sand related to the blowout and to improve the understanding of what factors affect the amplitude anomaly.

For seismic interpreters, one of the most difficult challenges is to deal with seismic resolution limitations. Geological events where are less than or closer to a quarter of the seismic wavelength cannot be accurately interpreted. Seismic amplitude is affected by tuning effect due to the interference of two seismic events related to the thinning of a geological layer. A full understanding of AVO tuning analysis is a prerequisite to conduct further analysis, especially for a thin reservoir. Tuning analysis in this thesis is addressed mainly through theoretical study, synthetic wedge modelling, relative amplitude analysis, and estimation of sand thickness.

Before AVO attributes and tuning analysis, the near stack and far stack data need to be balanced correctly by applying scalar factor. To check the feasibility of balanced data, a cross-plot of near stack versus far stack data is performed focusing on the shallow area.

AVO attributes analysis is conducted to help identifying the classification of gas anomaly. The construction of wedge model is based on the variations of gas saturation and reservoir thickness. The resulted tuning curves (relative amplitude as a function of thickness) need to be normalized for different saturation scenarios and offset partial stackings (near and far stack). The available well showing a thin gas sand in the area is below tuning thickness, and the calculation of sand thickness from amplitude also provide information about target areas where sands are expected to be thinner than tuning thickness. Thickness maps for different saturation scenarios and offsets are performed by linear regression calculation. By analyzing the relationship of amplitude and tuning thickness between the Near and Far stack, a feasible approach for implementing the discrimination of high amplitude caused by gas saturation and tuning effects is achieved at end. The seismic inversion model is also constructed to be a complementary tool for traditional AVO modelling in order to improve the interpretation.

2 Geological Framework

2.1 Location

The target area in the thesis is on the Steinbit Terrace in block 2/4 in the southern part of North Sea, where approximately 320 km southwest of Stavanger, as marked in the map. The water depth in the area is about 70-75 meters. It is located at approximately 57N 3E near the boundary of Central Graben, and the border between Norwegian sector and Danish Basin. The marked target well and the study area is shown in the Figure 2.1.

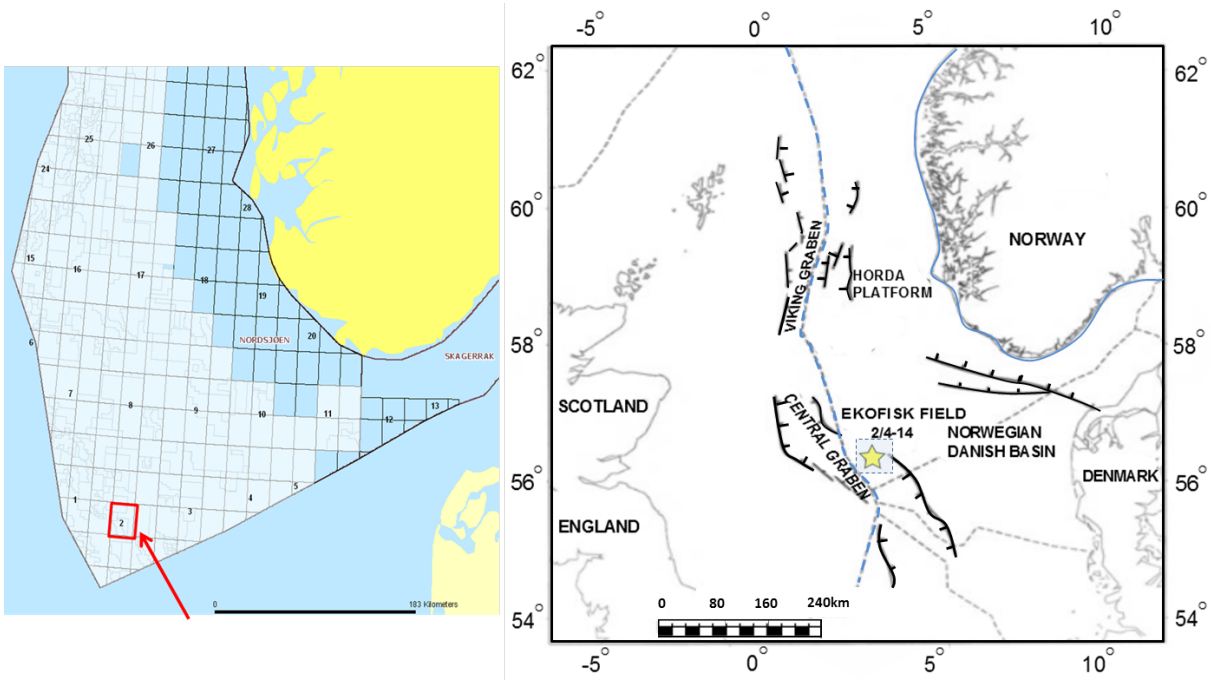

Figure 2.1: Location of target area on the left(Norwegian Petroleum Directorate). Main structural features, the boundary between national sectors and marked target well and area on the right.

2.2 Geological setting

Our target depth in this thesis is only the shallow parts within the upper 1Km beneath the seafloor. The uppermost group of the overburden is our target geological group, which belongs to Nordland Group. The upper part of this group consists of unconsolidated clays and sands, and contains occasional with larger ice-rafted detritus. It also discovered that the content with glacial deposits increase in the uppermost part of the group. (NORLEX, [2]).

Table 2.1: Major stratigraphic intervals from surface to deepest penetration in field (Modified version from [3])

Chronostratigraphy	Formation	Depth to Top in m subsea
Recent-Middle Miocene	Nordland Group	Surface to
Middle Miocene-Early Eocene	Hordaland Group	-1627
Early Eocene-Late Danian	Rogaland Group	-2761
Danian-Cenomanian	Chalk Group	-2889
Albian-Portlandian	Cromer Knoll Group	-3853
Ryazanian-Callovian	Tyne Group	-4043

Table 2.2: Major stratigraphic intervals from surface to deepest penetration in field (Modified version from [3])

The North Sea experienced several times during Quaternary age been partly or fully covered with ice sheet. During the glaciations, several erosion also was caused by the movement of ice sheets and melt water flow. It was acknowledged that the depositional environment in the target area is open marine with glacial deposits in the upper part. In the Norwegian Sea the Nordland Group was deposited in a marine environment in a rapidly subsiding basin characterized by major westerly progressing wedges. The upper part is of glacial to glacio-marine origin. (NORLEX, [2])

2.3 Blowout history

The gas and condensate discovery in well 2/4-14 crowned a challenging exploration story and led to an underground blowout. The underground blowout is referred as a special situation where fluids from high pressure zones flow uncontrolled to lower pressure zones within the wellbore. Usually, this comes from deeper higher pressure zones to shallower lower pressure formations.

In January 1989 Saga Petroleum drilled a deep exploration well in the target area. The primary objective was to assess the hydrocarbon potential of the main structure in block 2/4 (NPD fact-pages, [4]). The target was expected rotated Late Jurassic sandstone. When hitting the target, it encountered a high pressure zone, the drill bit got stuck and the well got kicked. A strong gas flow developed on the drill floor, and the blowout

preventer (BOP) on the seabed had to be activated. When the well was cut, it developed into an underground blow out, and then several attempts were made to gain control. A relief well 2/4-15S was drilled approximately 1.2 km to the south of the 2/4-14 well, based on the geological observations that illustrated that the shallow sand layers were slightly dipping to the north (Landrø, 2011, [5]). In the end, operator Saga Petroleum struggled for 14 months to deal with a sub-surface blowout in well 2/4-14. The underground blow out prompted Saga Petroleum initiating seismic monitoring the gas leakage for almost twenty years. This was considered to be the first successful 4D seismic acquisition offshore Norway (Landrø, 2011, [5]). Various surveys and analyses had been conducted to monitor any flow of gas into shallow formation. It is acknowledged that a large amount of gas migrated laterally, escaping into shallow thin sand layer locating at approximately 490m depth, which is our main target horizon (approximately 520ms). It is worth arousing great interest to do some further AVO analysis (Figure 2.2).

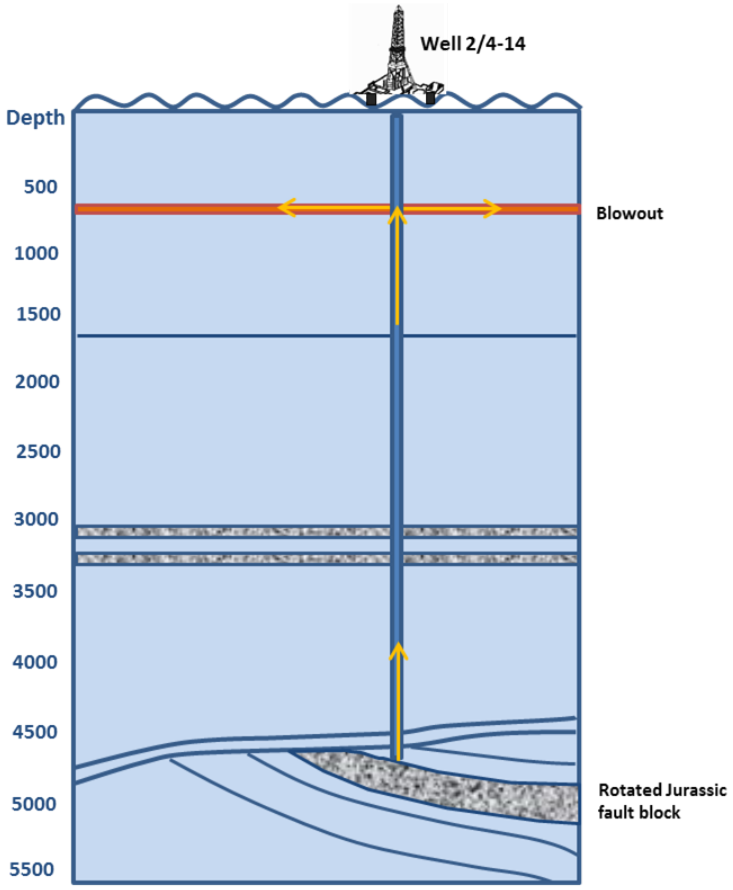

Figure 2.2: Sketch of the well 2/4-14 well blowout situation(Modified from [5]). The target depth is around 4500m in the rotated Juassic fault block, and also the yellow arrows represent the blow out into the shallow sand layers (Courtesy of Saga Petroleum).

3 Theoretical Framework

3.1 Amplitude versus offset

In 1984, Amplitude-verse-offset (AVO) analysis was initially proposed as a technique for validating seismic amplitude anomalies associated with gas sands when Ostrander published a break-through paper in Geophysics (Ostrander, 1984, [6]). He showed that the presence of gas in the sand overlaying by the shale would cause an amplitude variation with offset in pre-stack seismic data. The reduced Possion's ratio was associated with the presence of gas based on his discovery. Then, the year after, Shuey confirmed that Possion's ratio was most directly related to the offset-dependent reflectivity for incident angles up to 30 degree mathematically, as a classical approximation of Zoeppritz equation (Shuey, 1985, [7]). AVO technology, a powerful tool for hydrocarbon detection, started to show great advantages in oil industry combined with traditional qualitative interpretation.

Recent twenty years, AVO technique has became a very popular tool for hydrocarbon prediction, as one could physically explain the seismic amplitudes in terms of rock properties. Theoretically, AVO could be influenced by the contrasts in acoustic impedance and Poisson's ratio which are associated with the changes of fluid saturation However, the application of this tool need to consider some influencing factors, including thin bed effects, anisotropy and inelastic attenuation. Tuning effects have aroused great attention and interest in our thesis.

3.1.1 Offset-dependent reflection coefficient

Consider two semi-infinite isotropic homogeneous elastic media in contact at a plane interface. Then, an incident compressional plane wave impinges on this interface. A reflection at an interface disperses energy partition from an incident P-wave to a reflected P-wave, a transmitted P-wave, a reflected S-wave, and a transmitted S-wave as shown in Figure. 3.1 . The angles for incident, reflected, and transmitted rays at the boundary are related to Snell's law as:

$$p = \frac{sin\theta_1}{V_{P1}} = \frac{sin\theta_2}{V_{P2}} = \frac{sin\phi_1}{V_{S1}} = \frac{sin\phi_2}{V_{S2}} \tag{3.1}$$

where V_{P1} and V_{P2} are P-wave velocities, and V_{S1} and V_{S2} are S-wave velocities in medium 1 and 2, respectively. θ_1 is the incident P-wave angle, θ_2 is the transmitted P-wave angle,

ϕ_1 is the reflected S-wave angle, ϕ_2 is the transmitted S-wave angle, and p is the ray parameter.

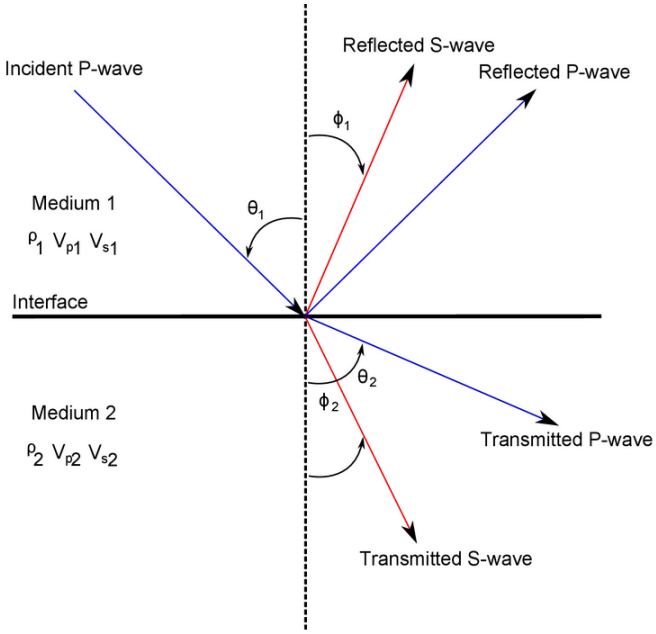

Figure 3.1: Reflected and transmitted waves at an interface between two elastic mediums for an incident P-wave.

Reflection coefficient is the ratio of amplitude of the reflected wave to the incident wave, or how much energy is reflected. At zero offset or normal incidence (Figure.3.2), there are not converted S-waves and the P-wave reflection coefficient R_0 is given by:

$$R_0 = \frac{I_{P2} - I_{P1}}{I_{P2} + I_{P1}} \tag{3.2}$$

where:

I_P = is the continuous P-wave impedance profile

I_{P2} = impedance of medium 2 = $\rho_2 \cdot V_{P2}$

ρ_2 = density of medium 2

I_{P1} = impedance of medium 1 = $\rho_1 \cdot V_{P1}$

ρ_1 = density of medium 1

3.1.2 Approximations of the Zoeppritz equations

The Zoeppritz (Zoeppritz, 1919, [8]) equations describe all possible plane wave reflection and transmissions coefficients at a plane interface as a function of reflection angle. The Zoeppritz equations allow us to derive the exact plane wave amplitudes of a reflected

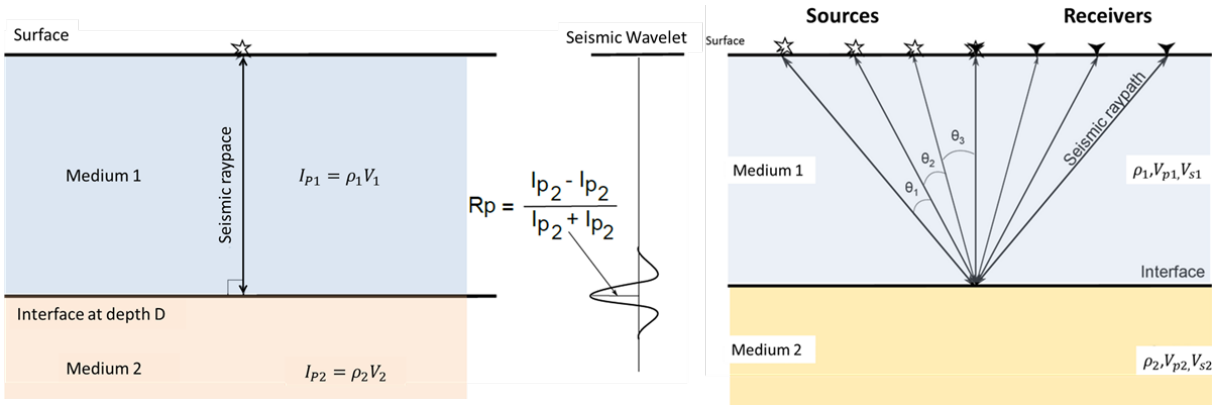

Figure 3.2: Zero-offset reflection coefficient is the difference of the product of the contrast of acoustic impedance at the interface of two different elastic mediums.

P wave as a function of angle, but do not give us an intuitive understanding of how these amplitudes relate to the various physical parameters. Over the years, a number of approximations to the Zoeppritz equations have been made. Among these approximations, some common and practical methods will be listed as follows.

The AVO technique has been developed by many researchers such as Ostrander and Rutherford and Williams (1989, [9]) and all of them were started from the Aki-Richards equation (Aki and Richards, 1980, [10]), which is a practical approximation to the Zoeppritz equation, assuming weak layer contrasts:

$$R(\theta_1) \approx \frac{1}{2}(1 - 4p^2 V_S^2)\frac{\Delta\rho}{\rho} + \frac{1}{2\cos^2\theta}\frac{\Delta V_P}{V_P} - 4p^2 V_S^2 \frac{\Delta V_S}{V_S} \tag{3.3}$$

where:

$p = sin\theta / V_{P1}$

$\Delta\rho = \rho_2 - \rho_1$

$\Delta V_P = V_{P2} - V_{P1}$

$\Delta V_S = V_{S2} - V_{S1}$

$\theta = (\theta_1 + \theta_2)/2 \approx \theta_1$

$\rho = (\rho_2 + \rho_1)/2$

$V_P = (V_{P2} + V_{P1})/2$

$V_S = (V_{S2} + V_{S1})/2$

In the equations above, p is the ray parameter, θ_1 is the angle of incidence, and θ_2 is the transmission angle; V_{P1} and V_{P2} are the P-wave velocities above and below a given interface, respectively. V_{S1} and V_{S2} are the S-wave velocities , while ρ_1 and ρ_2 are

densities above and below this interface as described in Chapter 3.1.1.

Shuey´s approximations of the Zoeppritz equations confirm mathematically that the Poisson's ratio is the elastic constant most directly related to the offset-dependent reflection coefficient for incident angles up to 30°:

$$R(\theta) \approx R_0 + G\, sin^2\theta + F\,(tan^2\theta - sin^2\theta) \tag{3.4}$$

where

$R_0 = 1/2(\Delta V_P/V_P + \Delta\rho/\rho)$
$G = 1/2 \quad \Delta V_P/V_P - 2\, V_S^2/V_P^2\, (\Delta\rho/\rho + 2\,\Delta V_S/V_S)$
$= R_0 - \Delta\rho/\rho\, (1/2 + 2\, V_S^2/V_P^2) - 4\, V_S^2/V_P^2\ \Delta V_S/V_S$
and
$F = 1/2 \quad \Delta V_P/V_P$

R_0 is the normal incidence reflectivity, G is the AVO gradient at intermediate offsets and F dominates the variation of the reflection coefficient at far offsets, near to critical angle.

Normally, the range of angles available for AVO analysis is around up to 40°, this simplifies Shuey approximation as follows:

$$R(\theta) \approx R_0 + G\, sin^2\theta \tag{3.5}$$

The contrast in acoustic impedance at an interface controls the zero-offset or incident angle reflection coefficient, R_0, while the gradient G varies with changes in density (ρ), P-wave velocity (V_P), and S-wave velocity (V_S) related to the rock properties. Koefoed (1955, [11]) first point out the importance of the Poisson's ratio or practical possibilities of the variations of V_P/V_S ratio in the offset-dependent reflectivity.

3.2 AVO attributes and cross-plot analysis

AVO crossplotting has been a standard tool for geophysicists since the 1990's, and many different techniques have been developed to better understanding AVO (Smith and Gidlow, 1987, [12]). The two factors that strongly determine the AVO behavior of sandstones reflections are the normal incidence reflection (R_0) called the intercept and the gradient

(G). These attributes can be analyzed by cross-plotting intercept (R_0) versus gradient (G). This display is a helpful and intuitive way of presenting AVO for a better understanding of the rock properties and fluid variations.

Equation 3.5 is linear if we plot R_0 as a function of $sin^2\theta$. We will then perform a linear regression analysis on the seismic amplitudes to estimate intercept $R_0(\theta)$ and gradient G. Before performing the linear regression, we need to transform our data from constant offset form to constant angle form. The general work flow is shown in Figure 3.3. A basic AVO analysis after appropriate geometric corrections, the individual traces for each gather is displayed in the panel on the left. The graph on the right shows one plot for time T2. The gay line is a least squares, a best fit to the natural distribution. The values for $R_0(\theta)$ and G are extracted from analysis of the best fit line.

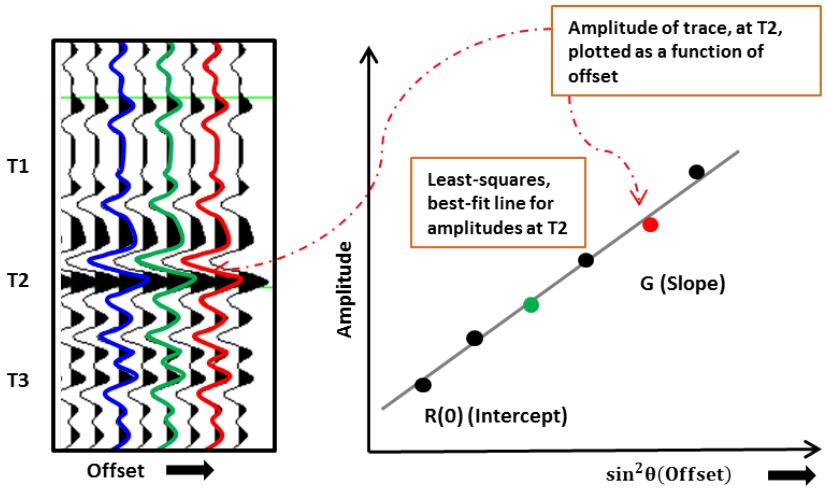

Figure 3.3: Sketch of general regression AVO analysis.

As shown in Figure 3.4, AVO cross-plot is split up into four quadrants, where the intercept (R_0) is along the x-axis and the gradient (G) is along y-axis. At the first quadrant (upper right), R_0 and G are both positive values. The 2nd quadrant is where R_0 is negative and G is positive (upper left). The third is where both R_0 and G are negative (lower left). Finally, the 4th quadrant is where R_0 is positive and G is negative (lower right). The quadrant numbers must not be confused with the AVO classes, as will be explained in detail further. These classes were originally defined for gas sands. However, nowadays the AVO class system is used for descriptive classification of observed anomalies that are not necessarily gas sands (Avseth et al.,2005, [17]).

Rutherford and Williams (1989, [9]) introduced a classification of AVO character-

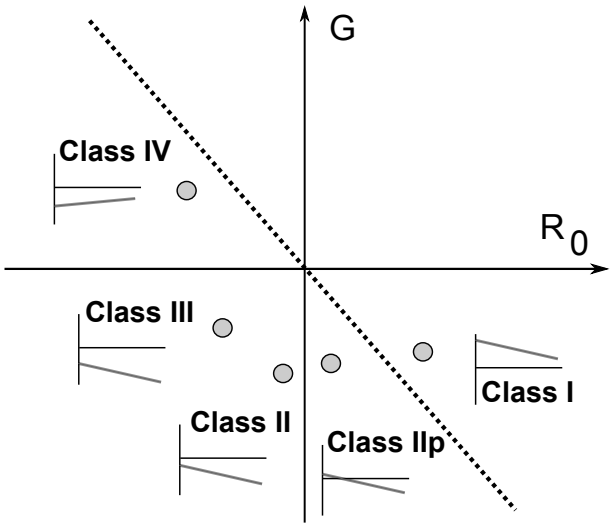

Figure 3.4: AVO cross-plotting, Rutherford and Williams AVO classes (1989), originally defined for gas sands (classes I, II and III), along with the added classes IV (Castagna and Smith, 1994) and IIp (Ross and Kinman, 1995). Figure adapted from Castagna et al. (1998).

istics for seismic reflections from the interface between shales and underlying gas sands. This classification is explicitly defined for gas sands and has become the industry standard. Three AVO classes are defined based on where the top of the gas sand is located in a R_0 versus G cross-plot (Figure 3.4). Table 3.1 summarizes the main characteristics of the different AVO classes. Class I are hard events with relatively high impedance and low V_P/V_S ratio compared with the cap-rock. Class II represent sands with weak intercept but strong negative gradient. Due to the low acoustic impedance contrast between the two layers, this kind of AVO class is often hard to see because they could produce dim spots on stacked seismic data. Class III is the AVO category that is commonly related to "bright spots". Class III sands are lower impedance than the overlying shales (classical bright spots), and exhibit increasing reflection magnitude with offset. The importance of this classification has been in demonstrating that reflection coefficients need not increase with offset for gas sands as was commonly assumed previously. In 1997, Castagna and Swan (1997, [14]) included a class IV AVO anomaly to the Rutterford and William classification scheme. The occurrence of this class is rare, but are produced by low acoustic impedance sands with gas capped by a relatively stiff cap-rock, such as a hard shale or tightly cemented sand.

The Rutherford and Williams classification for gas sands can be superimposed with

Table 3.1: AVO classification, after Rutherford and Williams (1989), extended by Castagna and Smith (1994), and Ross and Kinman (1995).

Class	Relative Impedance	Quadrant	R(0)	G	Amplitude vs. Offset
I	Higher than overlying unit	IV	+	-	Decreases
II	About the same as the overlying unit	II, III, IV	+ or -	-	Increase or decrease; May change sign
III	Lower than overlying unit	III	-	-	Increases
IV	Lower than overlying unit	II	-	+	Decreases

AVO intercept versus gradient cross-plot, as shown in Figure 3.5. It brings us more intuitive and better understanding of AVO classification. We have superimposed the left figure taken from Rutherford and Williams which shows their corresponding classification, while on the right normal incidence versus reflection coefficient displays. By closs-plotting, we can analyze the trends that occur in terms of changes in rock properties, including fluid trends, porosity trends, as shown with different arrows in the sub-left figure.

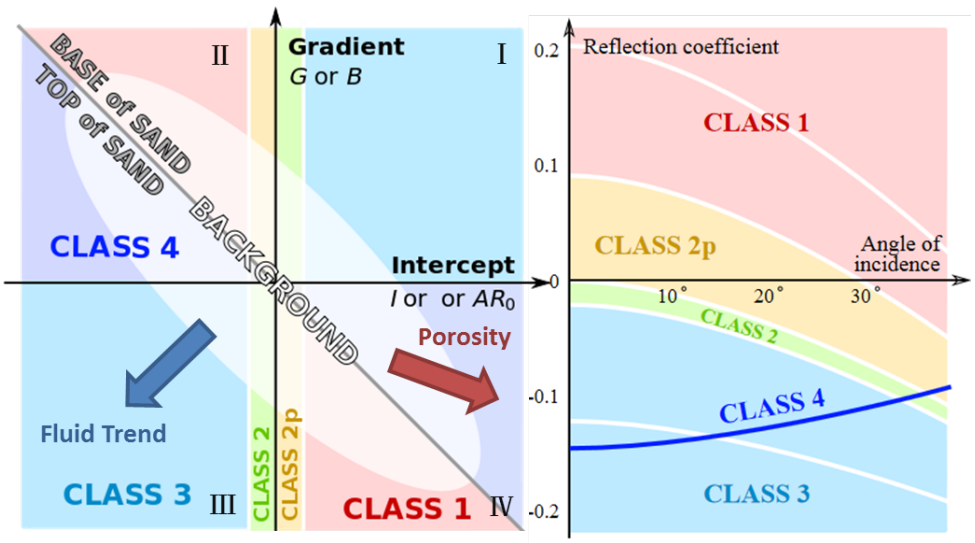

Figure 3.5: AVO cross-plot superimposed with reflection coefficient versus angle of incidence. Blue and red arrows are stand for fluid and porosity trend respectively.

Brine-saturated sands interbedded with shales is normally situated well defined 'background trend' in AVO crossploting (Castagna and Swan, 1997, [14]). A common and recommended approach in qualitative AVO cross-plot analysis is to recognize the

'background trend' before analysis other data points deviating from this trend. Castagna et al.(1998, [15]) proposed an excellent framework for AVO gradient and intercept interpretation. The base of sands will normally plot in the 2nd quadrant, with negative R_0 and positive G. The top of sands will plot in the 4th quadrant, with positive R_0 and negative G. The base and top of sands, together with background trends, create a well-shaped ellipse with center in the origin of the R_0-G coordinate system. It was derived hydrocarbon trends that would be nearly parallel to the background trend, but would not pass through the original cross-plots. For both soft and hard sands, we expect the top of hydrocarbon-filled rocks to plot on the left side of the background trend, with lower R_0 and G values compared with the brine-saturated case. Fluid trend can be marked as blue arrow in Figure.3.5, with the direction from brine to gas.

By using Shuey's two-term approximation to the Zoeppritz equation shown in Equation 3.5, it is possible to find a linear relationship between the AVO gradient and the far-near stack data. If we assume that far stack is around 30° and the near stack is at 0°. This is possible since the far stack normally will be representative for slightly lower angles than 30°, while the near stack will be representative for angles that are somewhat higher than 0°. When these two assumptions are fulfilled it is possible to derive an approximate relationship between the AVO gradient and the far-near data (Avseth, Dræge, et al. 2008, [16]):

$$Far - Near = R(30) - R(0) = G * sin^2 30 = G * 0.25 \tag{3.6}$$

3.3 Shear wave estimation

The shear wave profile is the key parameter controlling dynamic response characteristic of AVO behavior. A sound estimation of shear wave velocity is extremely important when shear wave data is not usually to acquire during the well logging. Shear wave could be calculated by two classical equations. Inside the reservoir, based on Greenberg-Castagna method, Vs is estimated by iterative calculations using different coefficient for each mineral constituent. Generally, Greenberg-Castagna iterative method is applied only to samples in selected reservoir zone, which matches zone conditions.

$$V_s = aV_p^2 + bV_p + c \tag{3.7}$$

For sandstone, the regression coefficients $a = 0$, $b = 0.80416$, $c = -0.85588$. Both Vp and Vs are in Km/s.

$$V_s = 0.8042V_p^2 - 0.8559V_p \tag{3.8}$$

Castagna's equation is applied when the mud rock line predicts systematically lower Vs. It is best suited for the more shaly samples, which usually calculate inside reservoir.

$$V_s = 0.862V_p - 1.1724(Km/s) \tag{3.9}$$

3.4 Rock physics analysis

Rock Physics establishes a link between the elastic properties and the reservoir properties such as porosity, water saturation and clay content. Rock physics diagnostic models and Gassmann fluid substitution relations are essential ingredients in generating the templates for a reservoir. Rock Physics Templates (RPTs) are geologically constrained rock physics models that serve as tools for lithology and fluid prediction (Avseth et al., 2005, [17]). In this section the basic rock physics concepts and models used for this thesis will be discussed.

3.4.1 Rock physics models

If velocity of a rock is predicted only with the porosity, the mineralogical composition, and the elastic moduli of the constituents, the best estimations can be made are the upper and lower bounds of the velocities.

The rock physics models are the link between rock physics properties and sedimentary microstructure. For this thesis, the friable- (unconsolidated) sand model was applied for the rock physics modeling. Schematic depictions of three major rock physics models are displayed in Figure 3.6.

The friable-(unconsolidated) sand model

This model for unconsolidated sediments assumes porosity reduction from the critical porosity due to the deposition that result in gradual stiffening of the rock. This porosity reduction for clean sandstone is caused by depositional sorting and packing. The elastic moduli at the critical porosity end point (ϕ_c) are given by Hertz-Mindlin (HM) theory. The zero porosity point represents the mineral point. These two points are connected by the unconsolidated line represented mathematically by the modified lower

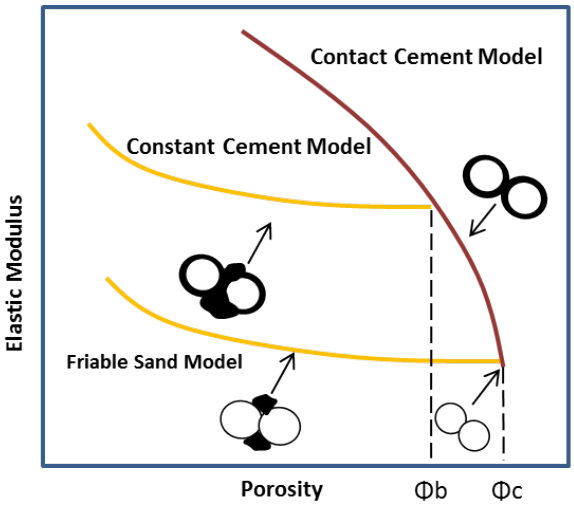

Figure 3.6: Sketch of three common effective-medium models. Modified from [17].

Hashin-Shtrikman bound (Dvorkin and Nur, 1996, [18]). It is more commonly appropriate for the shallow unconsolidated depth.

3.4.2 The Voigt and Reuss bounds

Voit (1910, [19]) and Reuss (1929, [20]) are the simplest upper and lower bounds respectively. The Voigt upper bound on the effective elastic modulus, M_V, of a mixture of N material phases is:

$$M_V = \sum_{i=1}^{N} fi \cdot Mi \tag{3.10}$$

where fi and Mi are the volume fraction and the elastic modulus respectively of the ith constituent. This is the stiffest bound which is the arithmetic average of the constituent moduli. This bound is assumed all the constituents have the same strain, and also called the isostrain average.

The Reuss lower bound of the effective elastic modulus (M_R), is:

$$\frac{1}{M_R} = \sum_{i=1}^{N} \frac{fi}{Mi} \tag{3.11}$$

This is the softest bound which is the harmonic average of the constituent moduli. For this bound is assumed all the constituents have the same stress, and also called the isostress average.

For both Voigt and Reuss formulas, M can represent any modulus. However, it is

more common to calculate this bounds averages of the shear modulus, μ and the bulk modulus, K, and then compute the other moduli applying the rules of isotropic linear elasticity.

3.4.3 Fluid substitution

Gassmann's (Gassmann, 1951, [21]) equations predict how the rock modulus changes with a variation of the pore fluids. The two fluid effects that are considered in the fluid substitution estimation are the change in rock bulk density, and also in rock compressibility.

The compressibility of a dry rock can be defined as the sum of the mineral compressibility and an extra compressibility due to the pore space, as follows:

$$\frac{1}{K_{dry}} = \frac{1}{K_{mineral}} + \frac{\phi}{K_{\phi}} \tag{3.12}$$

where ϕ is the porosity, K_{dry} is the dry rock bulk modulus, $K_{mineral}$ is the mineral bulk modulus, and K_{ϕ} the pore space stiffness. In the same way, the compressibility of a rock saturated with a fluid is defined as:

$$\frac{1}{K_{sat}} = \frac{1}{K_{mineral}} + \frac{\phi}{K_{\phi} + K_{fluid} \cdot K_{mineral}/(K_{mineral} - K_{fluid})} \tag{3.13}$$

where K_{fluid} is the pore-fluid bulk modulus. From Eqs. 3.12 and 3.13 Gassman's equations can be expressed as:

$$\frac{K_{sat}}{K_{mineral} - K_{sat}} = \frac{K_{dry}}{K_{mineral} - K_{dry}} + \frac{K_{fluid}}{\phi \cdot (K_{mineral} - K_{fluid})} \tag{3.14}$$

and

$$\mu_{sat} = \mu_{dry} \tag{3.15}$$

Therefore, Equations. 3.14 and 3.15 predict the modulus for an isotropic rock where the rock bulk modulus will change if the fluid changes, but the shear modulus will not. The dry and saturated moduli, are related to P-wave velocity as:

$$Vp = \sqrt{\frac{K + (4/3) \cdot \mu}{\rho}} \tag{3.16}$$

and S-wave as:

$$Vs = \sqrt{\frac{\mu}{\rho}} \tag{3.17}$$

where bulk density is estimated from:

$$\rho = \phi \cdot \rho_{fluid} + (1 - \phi) \cdot \rho_{mineral} \tag{3.18}$$

Fluid effects on wave velocities are shown in Figure. 3.7. The lower curve is for uniform saturation. It is characteristic by dropping dramatically with only a little gas saturation. This resulting bulk and compressional moduli will remain close to those of gas-saturated rock except for a narrow water saturation range near S_w =1. The upper curve is for patchy saturation with zero irreducible water saturation and zero residual gas saturation. The intermediate curve is for patchy saturation with irreducible water saturation 0.45 and zero residual gas saturation. The three theoretical curves are computed from the dry-rock data applying the Mavko et al method(1995, [22]).

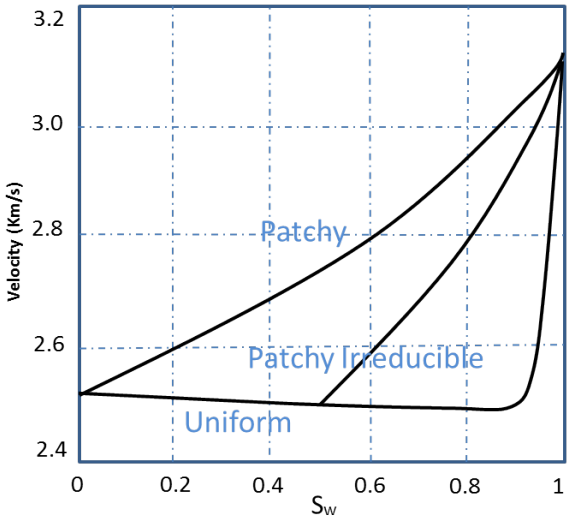

Figure 3.7: P-wave velocity versus water saturation for different saturation conditions. These three theoretical curves are computed from the dry-rock data applying the Mavko et al method (1995, [22]).

Gassmann's equations are applicable for mono-mineral rocks and from one pure saturation to another. And for homogeneous mixed fluid saturation (Resuss Average or Uniform), average bulk modulus and density of the effective fluid is estimated by using the following relations.

$$\frac{1}{K_{fluid\_avg}} = \frac{S_w}{K_w} + \frac{S_o}{K_o} + \frac{S_g}{K_g} \tag{3.19}$$

For the big patchy situation, Voigt limit is applied shown in the Eq. 3.20

$$K_{fluid\_avg} = S_w K_w + S_o K_o + S_g K_g \tag{3.20}$$

$$\rho_{fluid\_avg} = S_w\rho_w + S_o\rho_o + S_g\rho_g \tag{3.21}$$

S_w, S_w, S_w are the saturations, K_w, K_o, K_g are the bulk modulus and ρ_w, ρ_w, ρ_w are the densities of the brine, oil and gas phases respectively.

3.4.4 Rock physics templates

The combination of the depositional trends, rock physics models and fluid substitution in templates is what is known as rock physics templates (RPTs). This technology was first presented by Ødegaard and Avseth (2003, [23]). One of the most common RPTs is acoustic impedance versus Vp/Vs ratio. This kind of analysis starts with log data and then extends to seismic data (e.g. elastic inversion) for prediction of lithology and hydrocarbons. For the construction of the RPTs, porosity-velocity trends for the expected lithologies are estimated using Hertz-Mindlin contact theory (Mindlin, 1949, [24]) for the high-porosity end member. The other end point is at zero porosity and has the bulk and shear moduli of the solid mineral. The two end points are connected by the modified Hashin-Shtrikman (Hashin and Shtrikman, 1963, [25]) bounds for mixture of two phases. The next step is to calculate the dry rock properties with the rock physics models and apply Gassmann´s relations for estimating the brine and hydrocarbon saturated rock properties assuming a uniform or patchy saturation.

These RPTs are constructed honoring the local geology of the study area. Lithology, mineralogy, burial depth, pressure and temperature are geological factors that are considered in the creation of these templates. When the field data (well logs in our project, elastic seismic inversion not available) are superimposed on the template, different geologic trends can be identified in the data (Figure. 3.8).

3.5 Tuning effect on the AVO response

3.5.1 Theory

The AVO technique proved successful in some areas of the world, but in many cases it was not successful. The technique suffers from ambiguities caused by a thin-bed tuning, offset-dependent tuning, and NMO stretch among others (Avseth et al., 2005, [17]). Also some research results indicate, except for class I AVO reflectivity, AVO effects are significantly

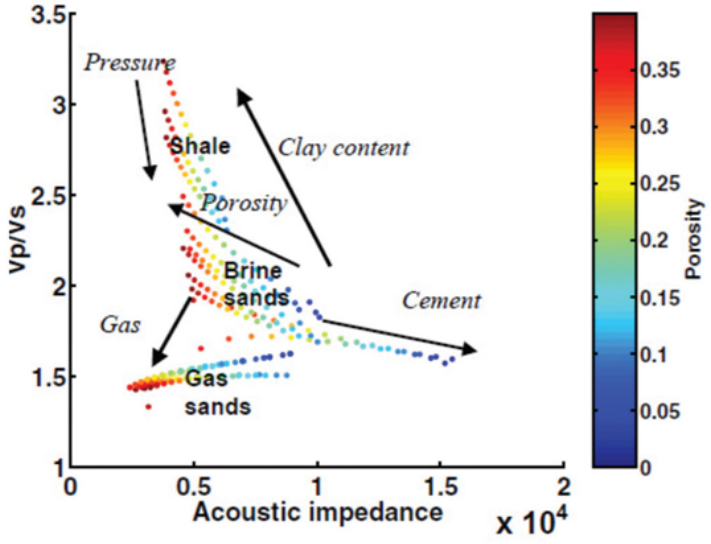

Figure 3.8: Rock physics template (RPT) presented as cross-plot of Vp/Vs versus acoustic impedance created by Matlab including rock physics models locally constrained by pressure, critical porosity, mineralogy, porosity, and fluid properties. The black arrows show various geological trends conceptually. The color legend represents the values of porosity.

altered by tuning effects (Chung and Lawton, 1999, [26]).

The tuning effect occurs when two stratigraphically separated reflectors are so close to each other that the reflected wavelet from the lower reflector interferes with the reflected wavelet from the overlying reflector. If the bed is too thin, the two reflections overlap and become indistinguishable, reducing the two reflectors to one, as illustrated in Figure 3.9.

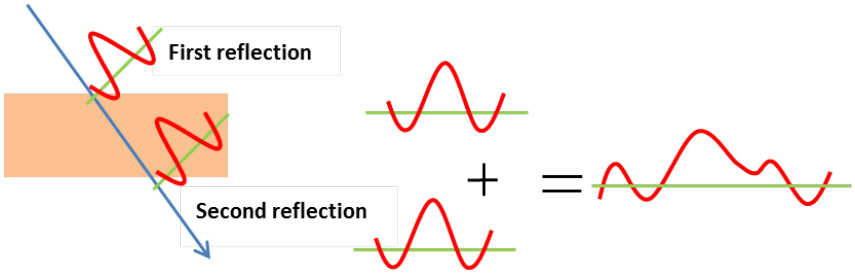

Figure 3.9: The principle of the tuning effects and wavelet

The tuning thickness is the thickness of that bed where tuning effects start to occur, as marked the dashed green line in Figure 3.10. Tuning effect start to happen if the layer thickness is less than tuning thickness, which almost equals to a quarter of wavelength (Widess, 1973, [27]). As tuning makes two reflected signals appear as either one signal

or even as no signal, this thickness therefore represents the limit of separability, where minimum bed resolution that the wavelet can identify. Figure 3.10 bottom shows the relative amplitude as a function of layer thickness for a given wavelength. It is observed that the amplitude starts to increase and becomes larger than the real reflectivity when the layer thickness below a half of wavelength. This is when we approach the maximum amplitude and observe constructive interference between the top and the base of layer. Furthermore, the amplitude decreases and approaches zero for layer thickness around one-eighth of wavelength and zero thickness (Charles and John, 2008, [28]). We refer to this as destructive interference. One-eighth of wavelength is also called the theoretical threshold of resolution according to Widess (1973, [27]), which is a limit of visibility. It is characterized by almost linear amplitude-thickness curve below $\lambda/8$ with decreasing amplitude as the layer gets thinner.

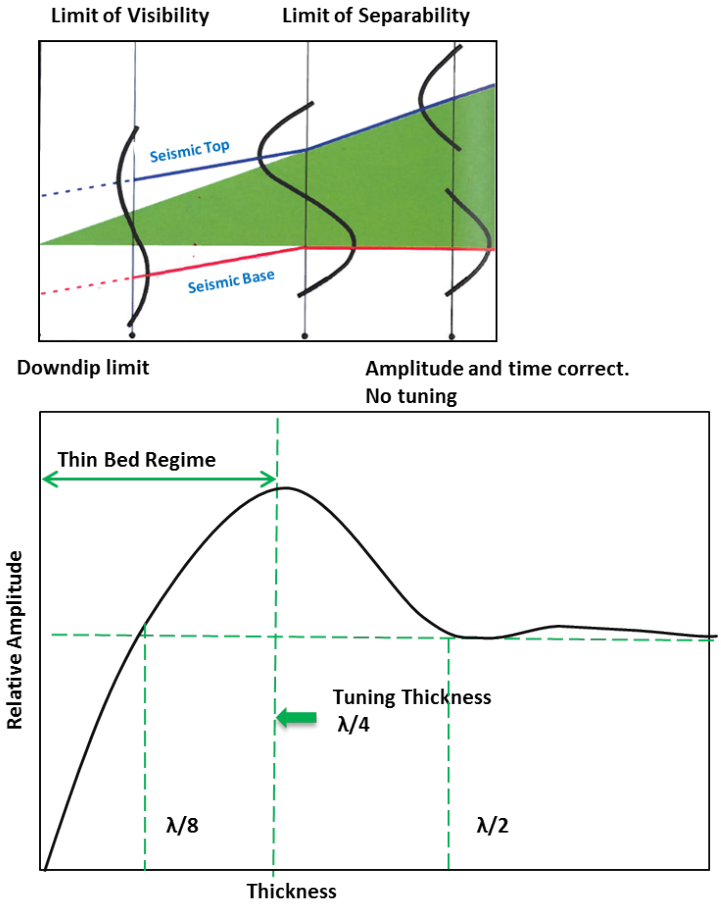

Figure 3.10: Tuning effects condition on the top. Seismic amplitude as a function of layer thickness for a given wavelength on the bottom.

It is significant to discuss how offset influences the tuning effect curves. Offset

dependency and NMO-dependency are main considering factors. Theoretically, greater offsets reduce the tuning thickness, as the differences between the bed's top reflection path and the bed's bottom reflection path becomes become less significant, as shown below. A simplified offset dependency effects model is built in Figure 3.11 below. Note that for a thin layer, t_1 is almost equal to t_2. The first zero offset reflection travels $2t_0$. The second zero offset reflection travels $2(t_0 + \Delta t_0)$. The first offset reflection travels $2t_1$. The second offset reflection travels $2(t_2 + \Delta t_2)$. According to the Pythagoras' theorem, therefore the time difference for the bed thickness is less for the greater offset. In fact, the amplitudes may interfere at large offsets even if they do not at small offsets.

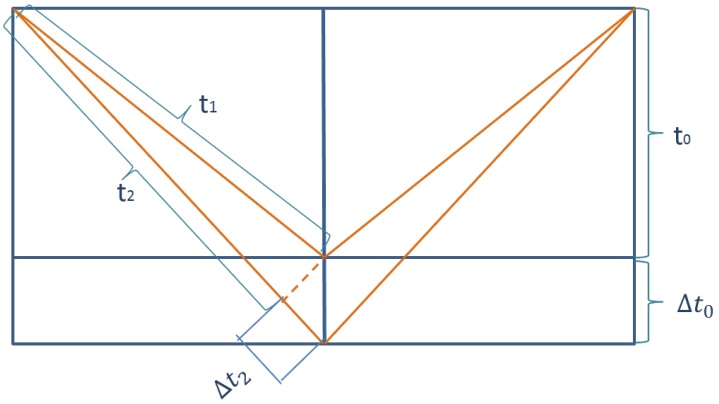

Figure 3.11: Simplified graphic representative of offset dependency effects. Modified from HampsonRussell.

However, since NMO stretching reduces the frequency of the wavelet at greater offsets, this leads to NMO Tuning. Even though tuning is inherent in the data before NMO correction, its effect on AVO is more obvious on NMO stretching data (Yong and Satinder, 2007, [29]). In practical, tuning is always affected by the wavelet frequency. A higher wavelet frequency gives a thinner tuning thickness and therefore better resolution. Due to the loss of higher frequencies caused by the NMO corrections, tuning thickness demonstrates the increase with offset.

3.5.2 Wedge modelling

Wedge Modelling is part of the AVO modelling tools. It can create seismograms to test how much the bed could thin before its top and bottom layer reflections interfere with each other. Through the wedge modelling, the thickness of sands will vary in order to simulate the response of tuning effect. The wedge model considered by Widess (1973,

[27]) involves two equal but opposite reflection coefficients, from the top and base of a thinning bed. When the bed thickness is large, the top-wedge and base-wedge reflections are separate. As the bed thickness decreases, the two events become closer together in time and start to interfere, forming a composite reflection event (Figure 3.12). Notice that this is a geometric effect and is independent of the fluid that is in the pores of the reservoir.

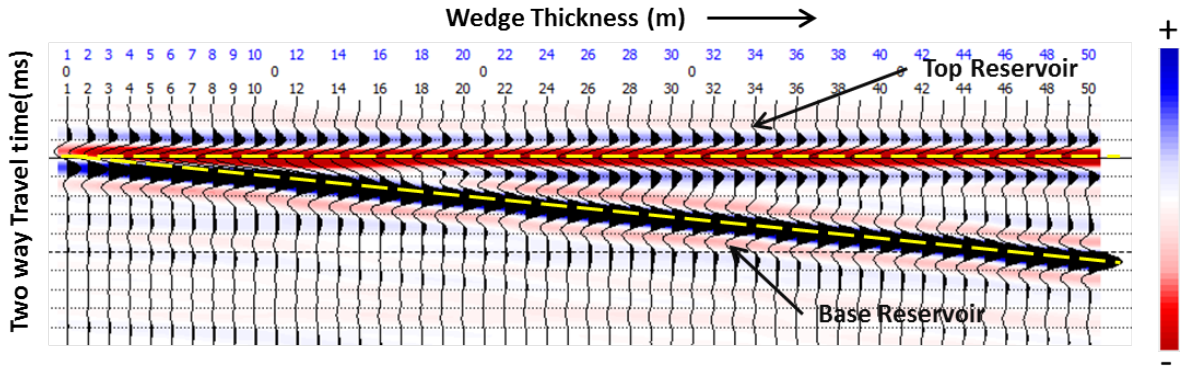

Figure 3.12: Simplified wedge model created by HampsonRussell, assuming common gas sands with the decrease of acoustic impedance. The yellow dashed line marked the top and base reservoir, which become closer together and start to interfere with the decreasing of bed thickness.

The general systematic can be changed by altering petrophysical or fluid parameter to see the predicted changes, while wedge modelling only changes the layer thickness. The basic log processing about wedge modelling is shown in Figure. 3.13. Only the yellow marked logs are modified to form the wedge shape. By fixing the top of the original well log, the logs above the top are not changed at all in this model, while the logs below the zone are shifted, but not change horizontally. This method uses the original time-depth curve to predict the times for the pseudo wells. Thickness changes in this model will represent new pseudo wells that can then generate new synthetic traces. These are "pseudo" wells as they have not actually been drilled or logged. These pseudo wells will have their own sonic and density logs and time-depth curves. This wedge process changes the logs for each modelled trace, and then calculates the model traces from those changed logs. Then the gathers of the wedge model can be applied analyzed in terms of amplitudes and AVO response of the target horizon.

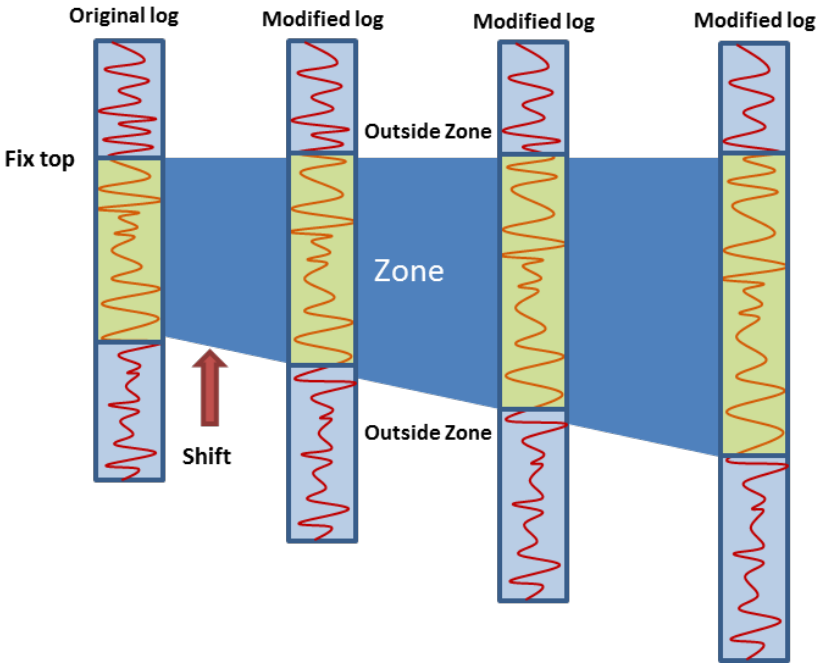

Figure 3.13: A synthetic wedge model with shifted from the bottom. These pseudo wells will be created to do further AVO responses, Modified from HampsonRussell.

3.6 Seismic impedance inversion

The process of seismic inversion is fundamentally based on the concept of identifying physical properties and features of underground rocks and materials. Inversion is the process of extracting from the seismic data, the underlying geology which gave rise to that seismic. Figure 3.14 shows a graphic description of modeling and impedance inversion processes.

In principle, the technique is very straightforward. If we assume that the seismic trace represents an approximation to the earth's reflectivity, then this reflectivity can be inverted to give the acoustic impedance. Figure 3.14 shows an acoustic impedance response from the earth which is convolved with a source wavelet to produce a resulting seismic signal which is measured. In principal, by deconvolving the source wavelet we could obtain the earth's reflectivity. Therefore, in practice, we could use inversion techniques to determine the seismic impedance, by removing the wavelet (treated as a bandpass filter) that comes from the acquisition and procession steps.

In this case, the first step for the inversion is to tie the well by comparing the synthetic trace and the nearest traces to the well location. The construction of the synthetic trace is necessary to use the wavelet extracted from the seismic data. A robust

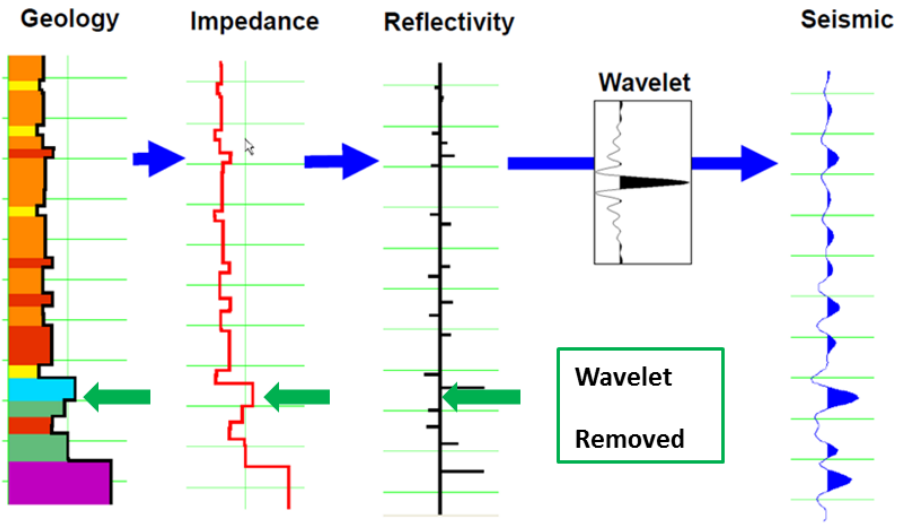

Figure 3.14: Principle sequence of seismic model and geology model.

method is to extract the amplitude spectrum from the seismic auto-correlation and use the well log to estimate an average phase. In this sense, inversion can also be considered a sophisticated method of integrating well logs and seismic data.

There are two main types of inversion currently being used. The first is band-limited inversion, which involves directly integrating the seismic trace. Since the seismic trace lacks a low frequency velocity trend because of the band-limited wavelet. We must therefore add in the low frequency component from the geological model.

The second type of inversion, which is more recent than the band-limited method, involves producing a "blocky" output rather than a band-limited output. There are several methods that produce this type of output, and they are sometimes referred to as sparse-spike or model-based methods. These methods work by producing a forward model that best reproduces the seismic data. Due to the non-uniqueness nature of the inversion algorithms, there is more than one possible geological model consistent with the seismic data. This method involves starting with a simple "guess" of this model and changing this guess iteratively until the error between the model and the observed seismic data is minimized.

4 Methodology

The post-stack seismic data provided by the company in 2005 and 2006 have been available as the sources of information for this thesis. These post stack data are well processed and stacked in near and far offset. The study area for this thesis covers around $240km^2$ in block 2/4 in the southern part of North Sea. At shallow depth, the available well logs in this area are limited. The only available well $2/4-16$ southeast 950m away from the blowout well $2/4-14$ was applied from the blowout area. The blowout well $2/4-14$ and relief well $2/4-15$ is approximately 1.2 km apart. Shown in Figure 4.1, target horizon with obvious gas anomaly arises our interest to do further research. In the following sections the programs used and the methodology applied for AVO attributes and tuning effects analysis will be described.

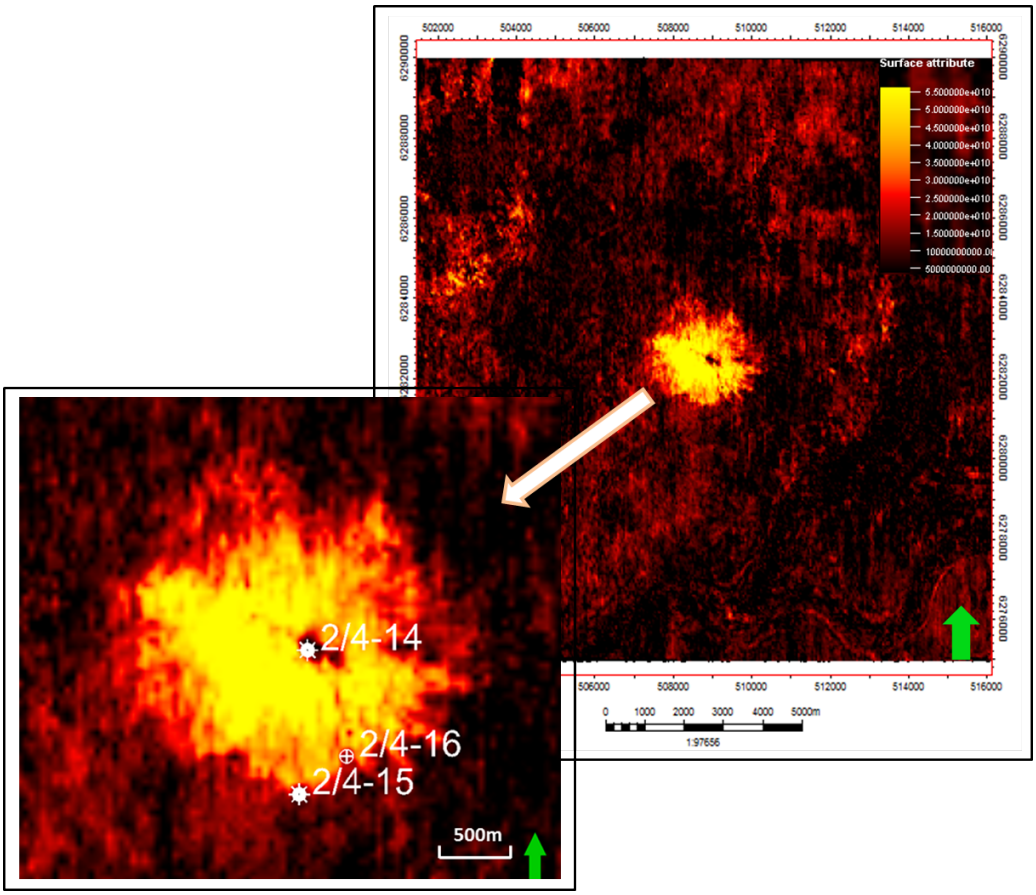

Figure 4.1: The whole area of 520ms and a close view on the left corner. The location of blowout well and nearby wells indicated by RMS amplitude extraction of target horizon 520ms from far stack seismic cube. Yellow color indicates high amplitude. Obvious gas anomaly was discovered on the target horizon.

4.1 Data description

Seismic data can have a large number of parameters associated with it. Reading those parameters from the seismic headers accurately is a crucial step. Some significant header parameters from both near and far stack are listed in the Table 4.1. Specific stack angle for different partical stacks had been defined and processed by the company. These parameters are extremely important when loading into the geological software, both in *Hampson-Russell* and *Petrel* Software.

Table 4.1: Near and far stack geometry parameters from seismic data headers.

Data Type	Near Stack	Far Stack
Stack Angle	3-14 degree	25-36 degree
Inline/Crossline	189/193	189/193
CDPX/CDPY	181/185	181/185
CDP	21	21
OFFSET	37	37

4.2 Software

The main programs were listed applying for data display, calculations and analysis. This thesis utilizes and alternates different programs to approach the objectives.

Matlab is a high-level programming software for data analysis, visualization, and numerical computation. In this thesis, this program was used for creating simplified wedge model to bring general idea before doing further research.

Hampson-Russell is a geophysical software specializing in AVO analysis, Seismic Inversion. The software suite brings intuitive seismic quantitative interpretation, and takes advantage of evaluating more data with less effort and getting better results. For this thesis, the data used in Hampson-Russell were well data and two data sets of post stack seismic to perform AVO analyses and to create wedge modelling together with synthetic seismic data based on information from the well.

Petrel Software Platform provides a complete solution from exploration to production, integrating geology, geophysics and geological modelling. Among these work flows, geophysics analysis is mainly applied in this thesis. Target horizon interpretation, am-

plitude analysis, RMS amplitude extraction and AVO cross-plotting were performed by Petrel.

Engauge Digitizer This open source, digitizing software converts an image file showing a graph or map, into numbers. The image file can come from a scanner, digital camera or screen shot. The numbers can be read on the screen, and written or copied to a spreadsheet. The final result is digitized data that can be used by other tools such as Microsoft Excel. It was applied to export the tuning effect curves into Excel to be edited afterwards, since *Hampson-Russell* do not have this operation.

4.3 Data quality control

The data quality control is significant when performing further analysis on seismic data. If the two stack data does have a certain scaled factor can result in wrong interpretations, to balance data correctly, and to perform the desired analysis.

After interpreting the target horizon, amplitude map shows intuitively that far stack has lower mean amplitude value than near stack. The seismic section has run in the opposite direction of our expectation that far stack should own higher values than near stack. In order to scale far stack more precisely, the corresponding amplitude extraction for both near and far stack were created by avoiding gas effect in shallower area and deep complex geological setting effects. Different seismic intervals were chosen to calculate the relevant mean RMS values to select more accurate scaled factor between near and far stack. (Table 4.2)

Table 4.2: Numerical calculation of the scaledfactor.

Seismic Interval [ms]	Near Mean RMS	Far Mean RMS	Far/Near	Average
$2250 - 3000$	1074473967	581128468	1.850	
$1000 - 3000$	1196441266	614310350	1.942	
$1750 - 2750$	1074558788	478514670	2.223	2

Through several attempts, scalar factor value 2 was determined to multiply by original far stack. It became more reasonable after balancing the two data set. As shown in Figure 4.2, the scaled far stack on the right side, as expected with higher amplitude, is well balanced with near stack on the left compared with the original data in the middle.

The full version is shown in the Appendix. Further RMS amplitude analysis for near, far and the difference between near and far will be discussed in the further section.

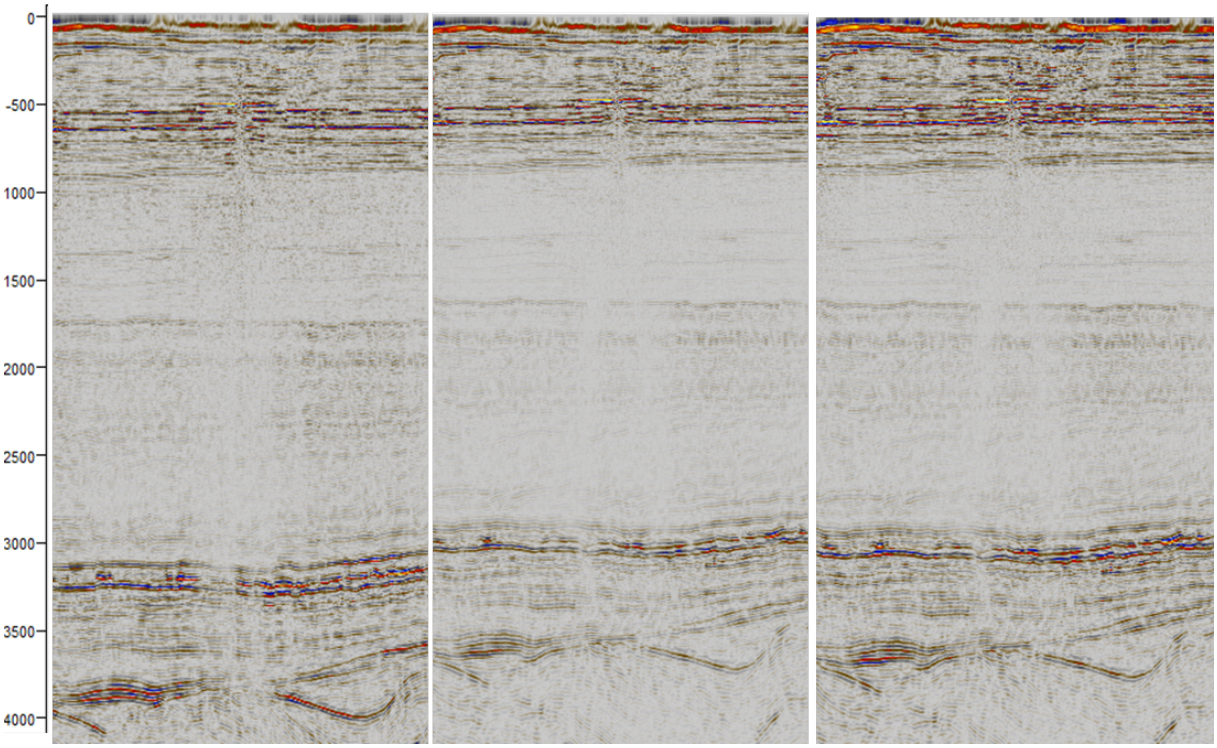

Figure 4.2: Near and far data set scaling. Left: Near Stack; Middle: Original Far Stack; Right: Scaled Far Stack.

To check the feasibility of balanced data, a cross-plot of near stack versus far stack data can be constructed in *Hampson-Russell* (Figure 4.3). However, if a cross-plot is made from the whole area, it will be some difficulties to distinguish the trends of hydrocarbon discoveries. The shallower part of seismic data (above 1000ms) was considered to be analyzed. What can be observed from this plot is that higher scaled far stack values is coherent with near stack values. The gray square in the center of Figure 4.3 was interpreted as a background tend with an angle of approximate 45 degree. To some degree, it means that the data were well balanced. The high amplitude zones marked as the red and blue circles can be highlighted as gas sands zone in shallow area. The corresponding seismic section is shown in Figure 4.4. The blue circle was displayed at the top gas in the seismic section, while the red one at base gas. Several thin gas sands can be discovered in shallow area as expected. The seismic section could provide a intuitive and rigorous view of thin gas sands around the target area.

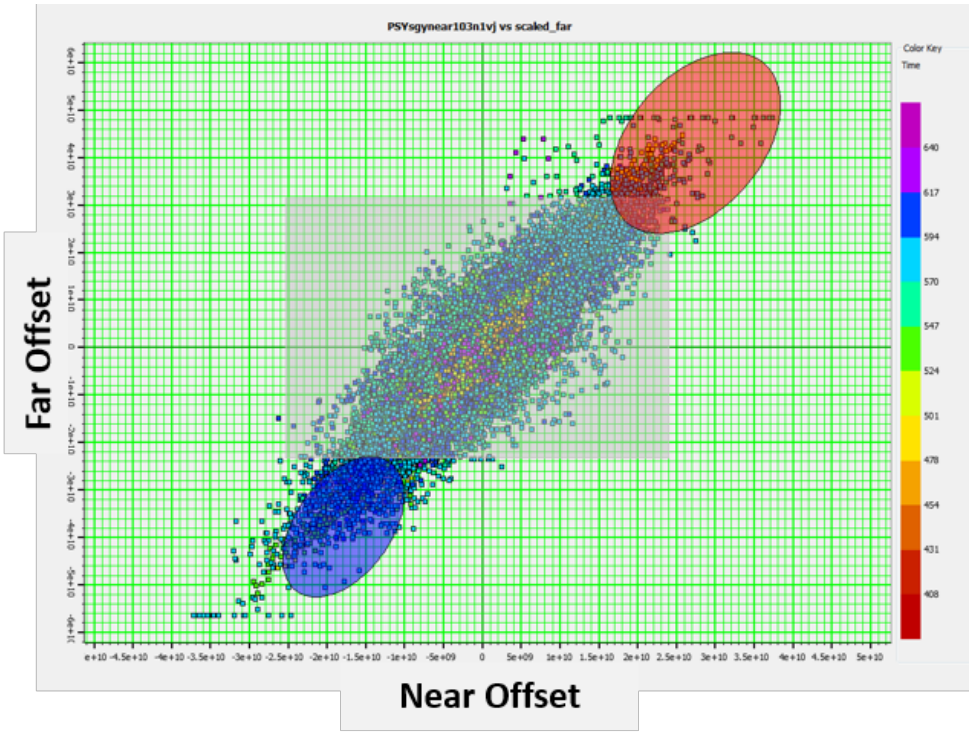

Figure 4.3: Cross-plot of near versus scaled far stack data. The color bar shows the two-way travel time. The gray square represent the shaly background trend, the red and blue circles represent the gas anomaly.

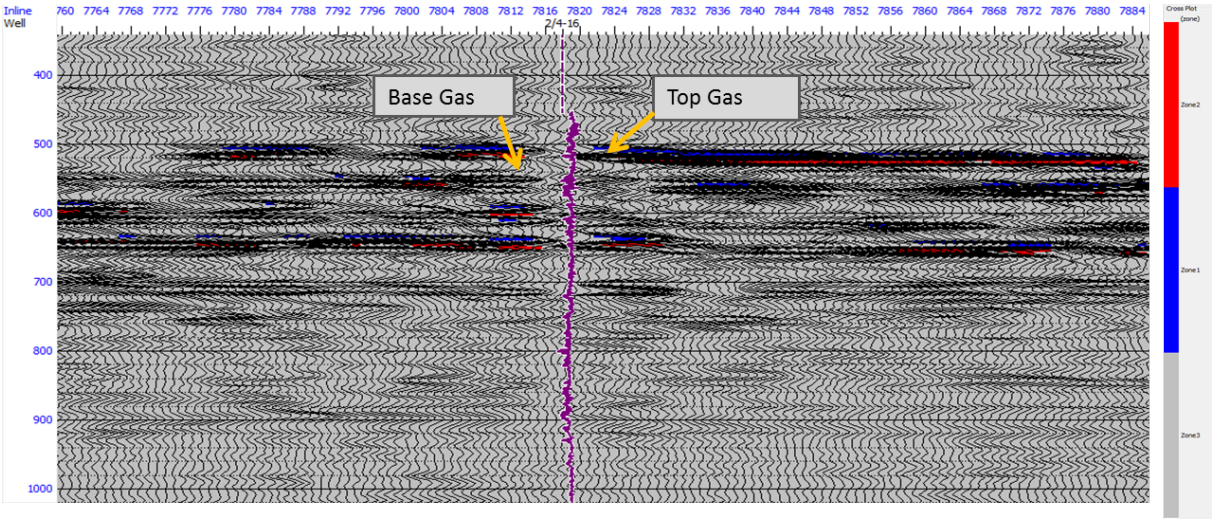

Figure 4.4: Relevant seismic section with the cross-plot. The color bar is corresponding to the circles color above. Major gas anomaly can be observed around the well bore which displays a purple line.

4.4 AVO attributes analysis

The objective of AVO attributes analysis is to identify hydrocarbon anomalies easier. After defining the best AVO attributes, further analysis can go further by differentiating between brine-filled rocks and hydrocarbon-bearing formations. To help with this, through the communication between visualization tools and the seismic data set, you can draw interest to anomalous regions for further study.

When pre-stack data is not available, partial stack data can be applied to obtain a good approximation of intercept and AVO gradient. The near stack data was used as an approximation of the intercept while the difference of far and near stack data can be used as an approximation to the AVO gradient. The background for this theory was found in the Chapter 3.2. For this attribute to be legitimate, both near and far stack data have to be correctly balanced (Avseth, Mukerji and Mavko 2005, [17]). A series of banlacing test were performed in Chapter 4.3, where it was found that the data are correctly balanced and then the cross-plotting was helpful, even with lack of pre-stack data.

Figure 4.5 shows AVO cross-plot that was created by geoboday Interpretation work flow in *Petrel*. The estimation of intercept and gradient cubes need to be normalized properly before cross-plotting. The cross-plot is robust (Right corner in Figure 4.5), and the background trend can be marked as blue dashed line according to Figure 3.5. The procedure of 3D geobody probe extraction will be shown in the Appendix. Once the highlight square in cross-plot was determined, an obvious gas anomaly on the target area (520ms) is shown in Figure 4.5. Panning through geological sequences using the horizon probe function, our target zone AVO anomaly distribution map (520ms) can be constructed easily. Based on AVO classification, our target horizon was characterized as class III anomaly, which is normally a 'bright spot' obvious shown in the seismic data. Since the class III AVO anomalies represent soft sands saturated with hydrocarbons, the classification made it fit well with this reservoir where there are unconsolidated sands in the shallower part. The extent of AVO anomaly is a comparable with the area of extracted high amplitude in far stack. Yet, the accurate calculation of them shows a slightly smaller extent in AVO cross plotting. The reason for this will be indicated in further section.

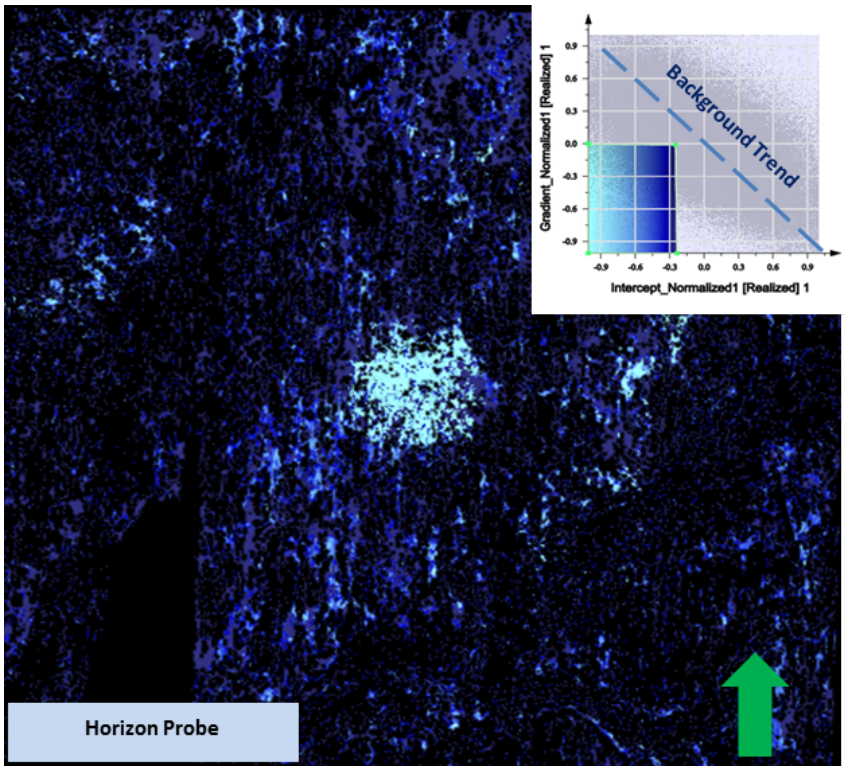

Figure 4.5: AVO cross-plotting is on the right corner, demonstrating class III anomaly. The target horizon displays a obvious gas anomaly in the center by applying horizon probe fuction in *Petrel*.

4.5 RMS amplitude analysis

The RMS (Root Mean Square) attribute emphasizes the variations in acoustic impedance over a selected sample interval. Generally the higher the acoustic impedance contrast of stacked lithologies (with bed thicknesses above the seismic resolution), the higher the RMS values will be. Therefore, RMS amplitude is effective technique to distinguish hydrocarbons, since hydrocarbon often has strong amplitude.

Figure 4.6 illustrates the comparison of our target horizon, seismic section and RMS amplitude extraction. On the left, the gamma ray log with lower values indicates around 7m target gas sand (512-518ms, corresponding to 490m MD in the well). 3D seismic section through the blowout well both Inline and Xline (two black dashed lines indicate on the right RMS extraction map) display a strong amplitude marked with white squares. It was observed a gas anomaly pull down from seismic inline. The horizontal extent is approximately $2.4Km$. A rough predicted extent of target shallow gas anomaly was approximately $3.7km^2$ by the identification of only high amplitude anomaly. Compared

to the previous research, the mapped extent of this gas anomaly from 1990 seismic 2D line is significantly less than $3Km^2$ (Landrø, M., 2011, [5]). One reason for this could be a indication of gas migration or any other inducing factors. Besides, a finger shape pinch-out pattern marked with a white circle is remarkable and interesting to note. It is also possible to consider as a result of tuning effect. Due to the poor calibration in shallow area, it brings out many difficulties and uncertainties to estimate the gas sand thickness. Further tuning analysis with the estimation of sand thickness will be conducted concentrating on this fingering shape horizon.

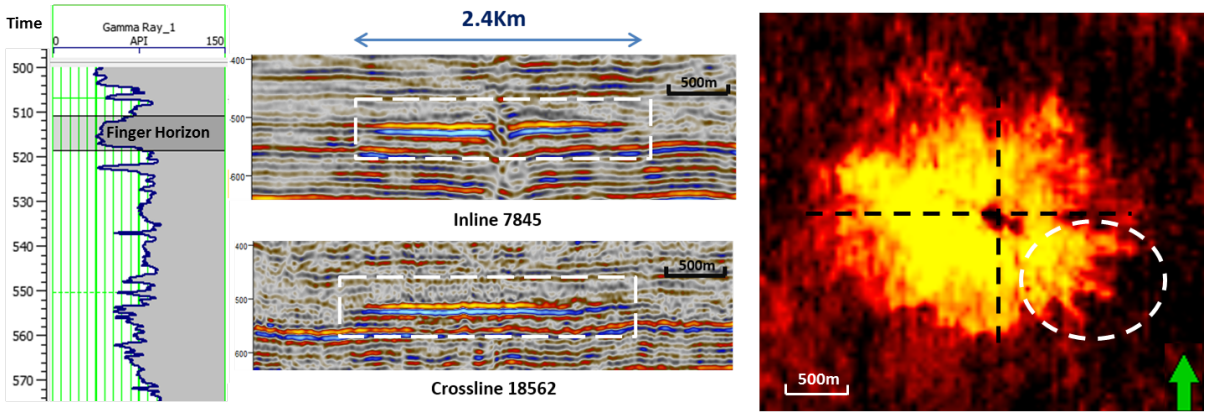

Figure 4.6: The target horizon description from the well log and seismic. Left: Gamma ray log displayed the target gas sand; Middle: Relevant 3D seismic Inline and Xline section, the white box displayed the area of high amplitude caused by blowout; Right: RMS amplitude extraction on the target horizon, the marked circle demonstrated an interesting fingering shape.

The gray color was set to control amplitude value below 1.5E+010 in order to display visually. Figure 4.7 shows the RMS amplitude extraction from target horizon (520ms) for both far and near stack. Keeping the same color scale, the amplitude extraction from the scaled far stack is much higher than the one from the near stack as expected. There is also worth noting the extent of gas anomaly from far stack is larger than that the one from near stack. Further analysis need to be conducted to distinguish the reason of amplitude anomaly marked white circles between tuning effect and gas content.

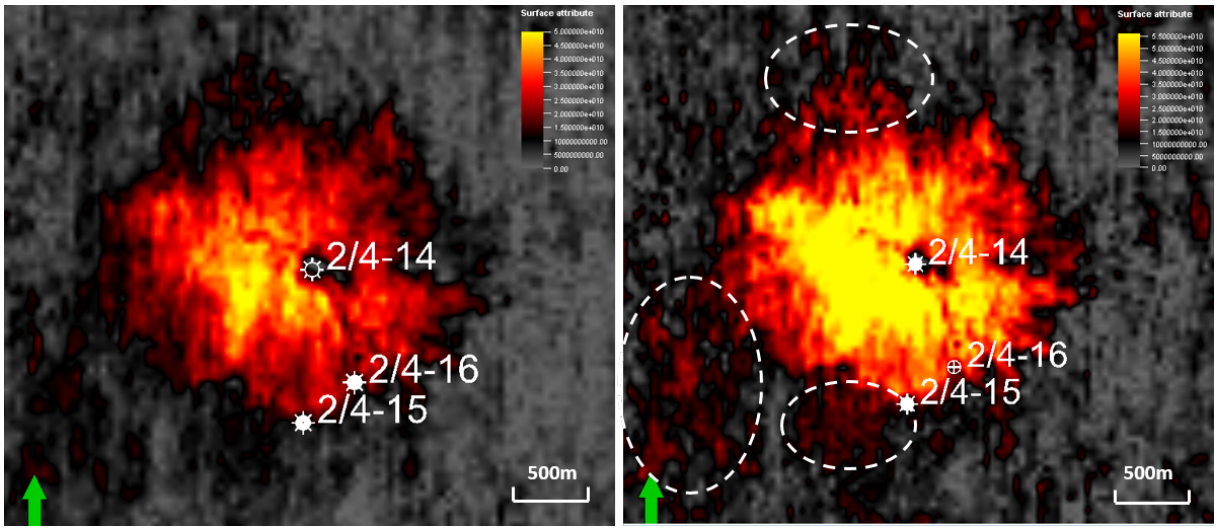

Figure 4.7: RMS amplitude extraction on the target horizon for both near stack and scaled far stack; The same color scale was set and yellow indicates high amplitude.

In order to analyze the distribution of the blowout area related to high amplitude, the color legend was changed to HSV colorful mode. RMS amplitude extraction for far stack is more easier to demonstrate a ring-shape amplitude distribution from the center of blowout area. In order to sustain our assumption, the plot of amplitude versus the extension from blowout well to the proceeding well 2/4-16 was applied as shown in Figure 4.9.

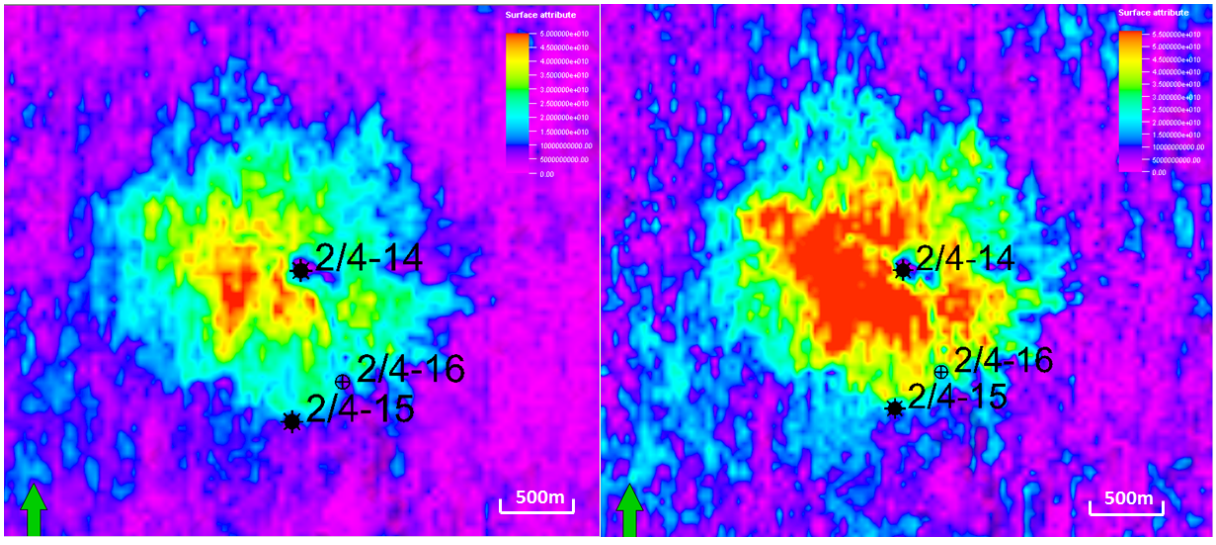

Figure 4.8: RMS amplitude extraction for far stack on the Finger horizon with the color legend.

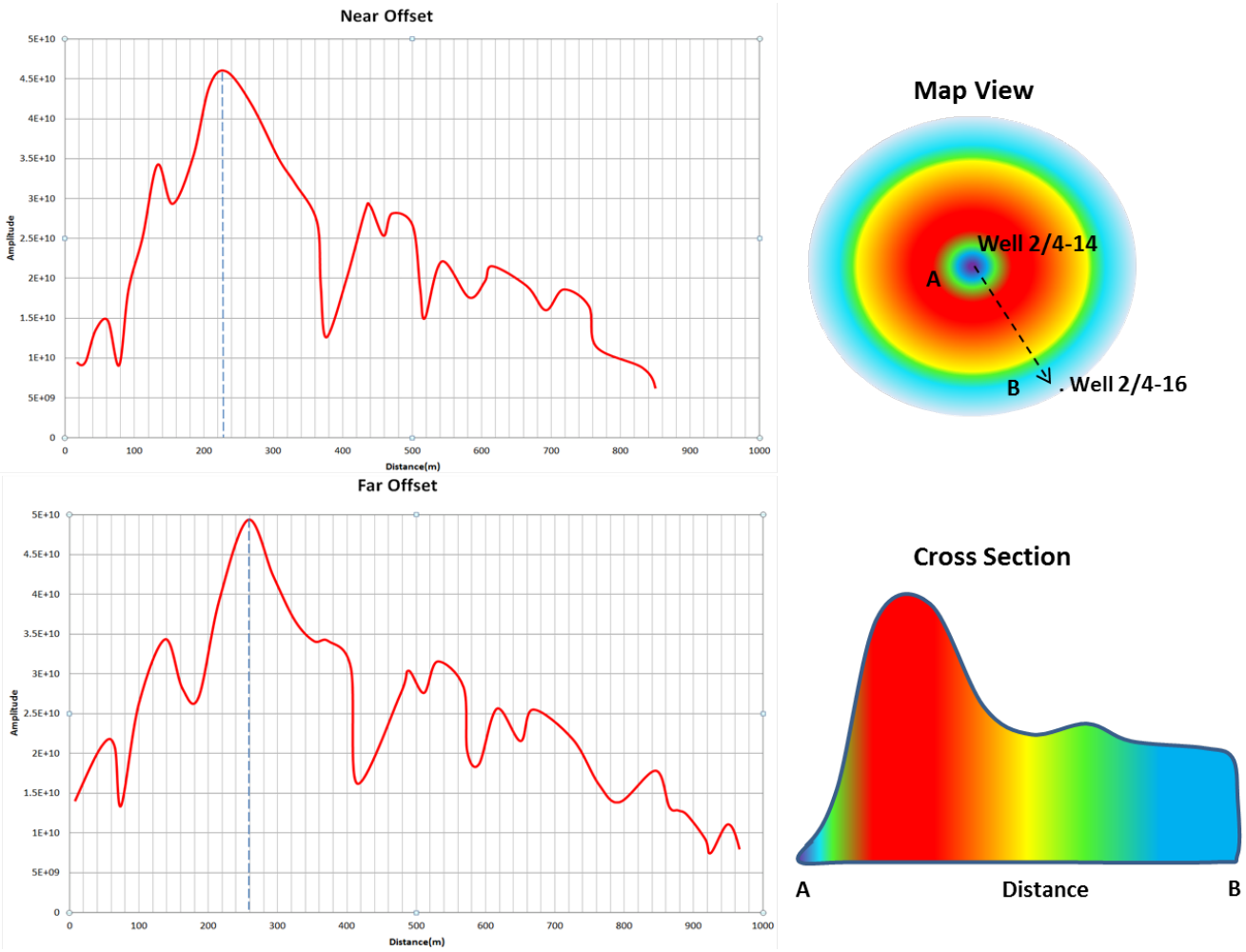

Figure 4.9: The plot of amplitude against the distance from blowout well to the available well 2/4-16, the largest amplitude was marked as a blue line. The sketch of ring shape amplitude distribution is shown on the right top, while the bottom profile of smoothing curve can be analogical with tuning effect.

Raw amplitude extraction of target line marked as a dashed black line from A to B was done in *Petrel*. The first step is to smooth the data curves to get rid of noise effects. By plotting amplitude against distance from blowout center to the border, the smoothed amplitude exhibited a jump increase around 250m apart from the blowout well. The dashed blue line was marked to display the highest value for both near and far stack. The far stack displays a slightly higher amplitude and a distance shift of approximately 35m compared with the near stack. In general, the amplitude experienced a dramatic increase around the blowout area, and then a second small peak was followed last for around 120m. A gradual decreasing occurred after 600m. The simple sketch of this annular amplitude effects in seismic section was displayed on the right top of the figure. The color legend is

corresponding to RMS amplitude extraction from far stack in Figure 4.7. The estimated smoothing curve with the corresponding color legend demonstrates a analogical shape with tuning effect. The profile gives some evidences of tuning effects as a main factor associated with high amplitude gas anomaly in the target horizon. The big differences of central fingering shape section between near and far is not only due to gas saturation, but also tuning effect could be associated with.

4.6 Wedge modelling

Wedge models with synthethic seismograms are created to analyze the predicted changes by altering a petrophysical or fluid parameter. Estimate seismic reflection responses across a thin bed is developing the principles of thin-bed interpretation. Further tuning analysis will be emphasized in this section.

4.6.1 A simplified wedge model

In order to investigate tuning effect, a simple wedge model with a constant impedance was created to simplify our case. The wedge depth is from 500m to 550m with the width of 50m. The assuming densities and P-wave and S-wave velocities of target layers from sea bottom to our target shallower area (800ms) were shown in Figure 4.10 top left. Relative reflection coefficient can be calculated by using Eq.3.1.1. The Ricker wavelets from near offset and far offset can be extracted from the zero phase-converted data from *Petrel*. The top right figure shows the wedge modelling after convolution. A relevant synthetic seismogram of wedge model created in *Hampson-Russell* was presented on the bottom of the figure. The polarity was shown as American polarity. In this model, the media above and below the thin bed have the same acoustic impedance, which causes the reflection coefficients at the top and bottom of the bed to have the same magnitudes but opposite algebraic signs, as marked yellow dashed line.

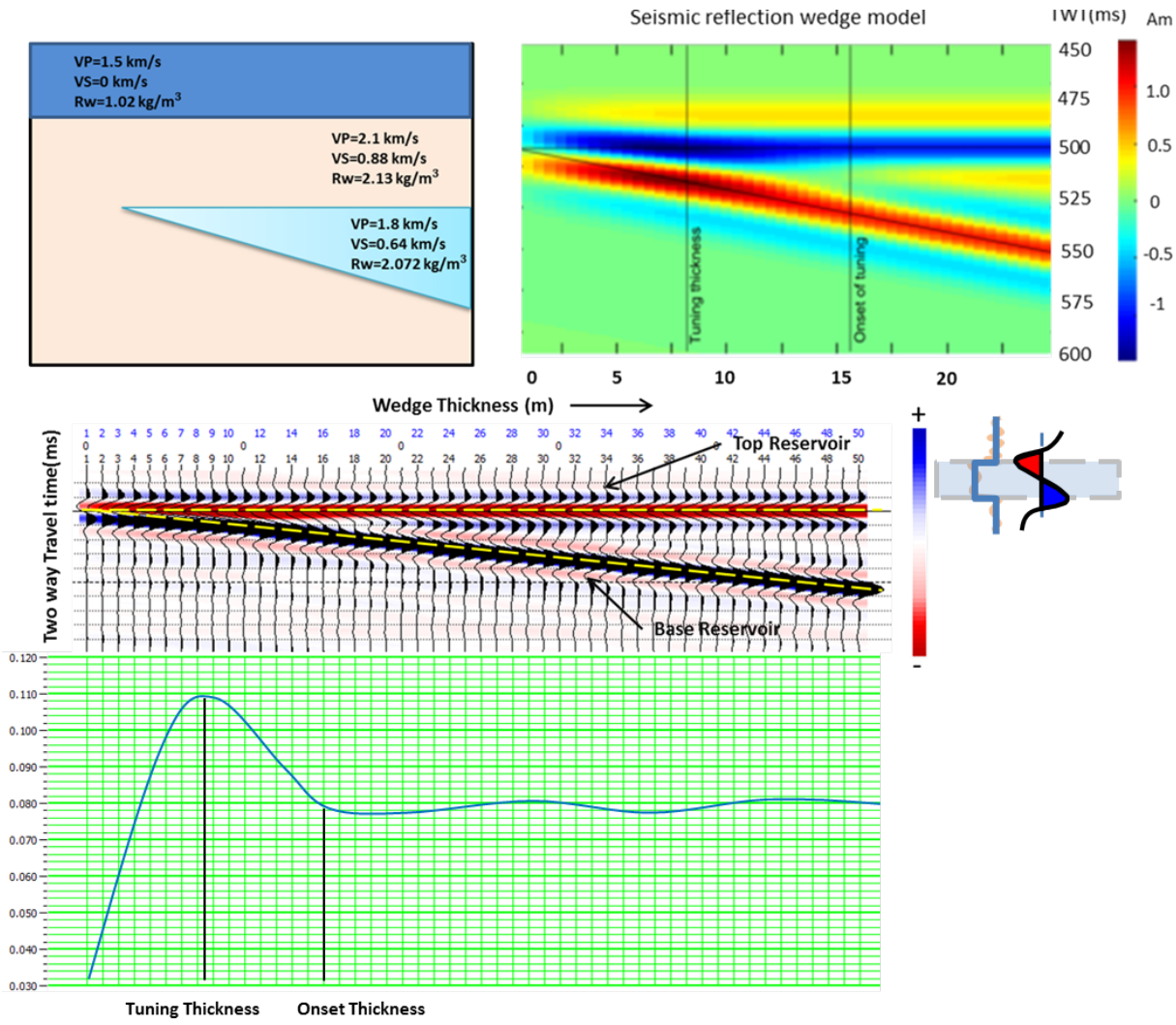

Figure 4.10: Rock properties of simplified wedge modelling on the top right. The corresponding synthetic seismic section of wedge model created by *Matlab* and *Hampson-Russell*.

The tuning curve shows the thickness along the top of the wedge (thin black lines in both seismic reflection wedge models in Matlab and HampsonRussell). The onset of tuning is the thickness at which the bottom of the wedge begins to interfere with the top of the wedge. This value brings the idea of the constructive amplitude period could have two possibilities of thickness.

4.6.2 Application to a real geological setting

In order to validate some of the observations made so far, a more advanced geological synthetic wedge modelling approach has been applied. Wavelet extraction and well ties are two important steps to construct the wedge model.

Wavelet extraction

To construct an accurate wedge model, the first step is to determine a proper seismic wavelet. Wavelet extraction from the data has been a challenge, since the noise in shallow area raises difficulties. The reason for choosing the wavelet from the seismic instead of wells is that log correlation errors can cause phase problems. The corresponding near and far statistical wavelet were shown in the following Figures 4.11, 4.12. Through some attempts for avoiding the lower band frequency for seismic, more reasonable time range for shallow target area is from 400ms to 1000ms since shallow area effects enormously. The major frequency range for both the near and far stack is around 45-50HZ. The extracted wavelet displayed its time response and frequency spectrum. This wavelet are used to create synthetic traces and wedge modelling afterwards.

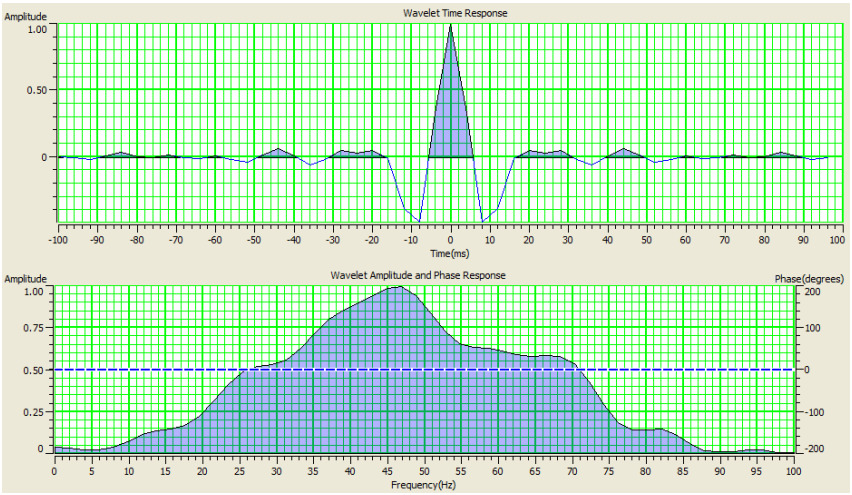

Figure 4.11: The wavelet extracted from near stack, from 400ms to 1000ms.

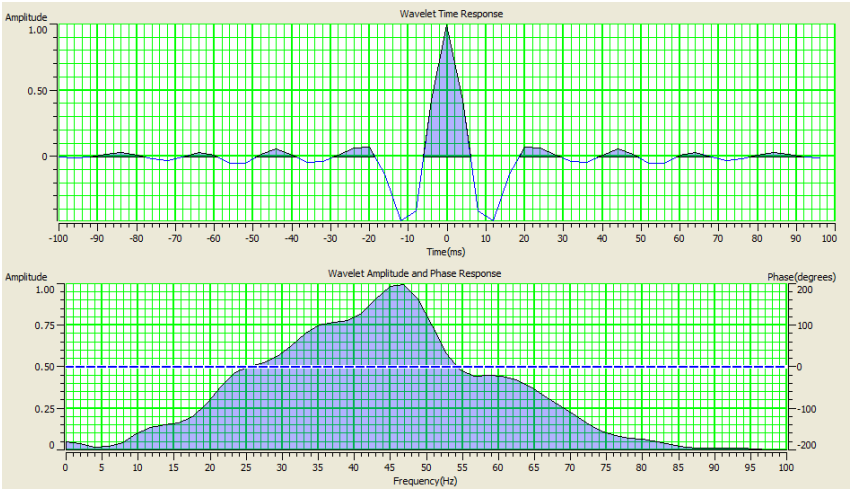

Figure 4.12: The wavelet extracted from far stack, from 400ms to 1000ms.

Well Correction

Another crucial step before further analysis is well tie. Log correlation is an important process of applying a manual correction to the well depth-time curve to optimize the correction between initial model and seismic data. The well data from well 2/4-16 was applied to get information and obtain a better understanding of seismic data. Correlation can be achieved by matching events on a well synthetic with the same events on a seismic trace at the well location.

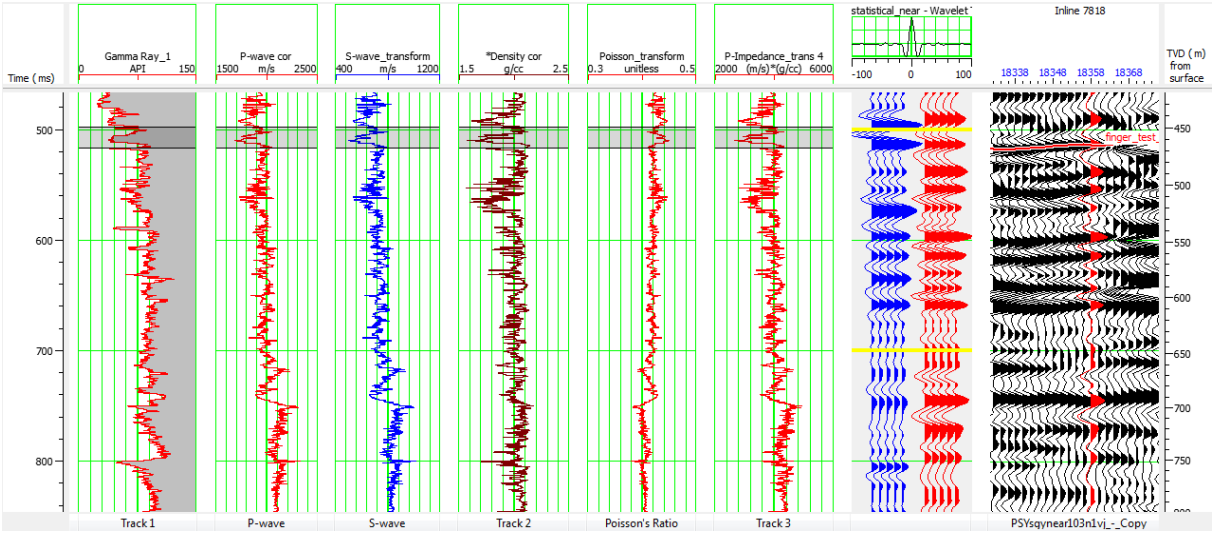

Figure 4.13: Well tie conducted in the well 2/4-16. From left to right: Gamma ray log, P-wave velocity, S-wave velocity, Density log, Calculated acoustic impedance and Vp/Vs ratio, the synthetic traces correlation.

Figure 4.13 shows the well logs after correction has been performed. All these logs contain invaluable information which can help defining our target shallow area more exactly. Our target area is marked as gray color. We notice this thin sand layer is characterised by low P-wave velocity and density. The last two logs Possion's ratio and acoustic impedance are logs that were computed in *Hampson Russell*. The well synthetic on the right displayed how the well match with the seismic. The blue synthetic trace represent the wells, while the red one stand for real seismic. The sonic log is then modified by the time shifts so that the synthetic and seismic time match. The log correlation is difficult due to the poor well calibration, especially in the shallow area. By applying a time shift and stretching on the shallow area (400ms-1000ms), the window shows a much improved correlation, maximum coefficient up to 0.62. The coefficient window is shown in the Appendix.

Wedge modelling and tuning analysis

The seismic survey geometry need to be defined and populated by interpolated mapping of measured well logs P-wave velocity, and density or modeled shear wave velocity. Changes in fluid situation and acoustic properties along with changes in bed thickness are introduced into the model determined synthetic gradient analysis. A synthetic seismic model is generated from wedge model by applying a range of wavelet.

Since shear wave is not available in well logs, a rock physics template was applied as a quality control. It was generated before the further wedge modelling analysis achieving the goals of more reasonable shear wave velocity. Outside the gas sand, based on the lithology and geological setting in our target area, Castagna's equation (Eq.3.9) is applied. While inside the gas sand, based on Greenberg-Castagna method, shear wave can be predicted by using Eq.3.8. For three different scenarios-water, patchy and uniform saturation (Eq.3.19, Eq.3.20, Eq.3.21) were applied respectively to estimate rock properties. The calculated logs of acoustic impedance and Vp/Vs ratio were used to create a rock physics template (RPT) plot as a quality control.

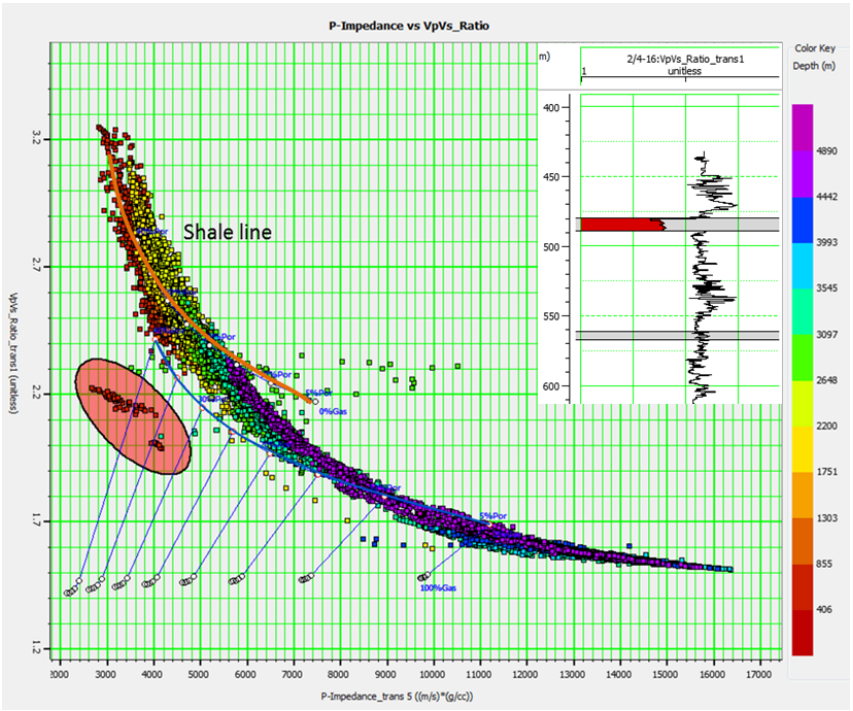

Figure 4.14: Rock physics template. Rock properties of simplified wedge modelling on the left. The corresponding synthetic well section of wedge model

The points in the figure above were plotted as a function of depth which is shown on the colourbar. The red highlight zone represented for shallow gas zone, which is

characteristic by low Vp/Vs and AI value. This zone is located at 490MD which is comparable with the log zones as expected (on the right corner of the cross-plot). Shales are composed of soft clay minerals and are normally not cemented in shallow depths, and an unconsolidated regime was assumed. Thus the friable-sand model was used for the shale line. From the cross-plot, shallower area are more shalely sands according to the trend of the shale trend. The purple color points below 4000m depth correspond to the cementated rocks. Some parameters were set to make the standard RPT (blue line) fit to main trend points. Effective pressure was calculated from the depth. K Modulus and G Modulus are respectively 37Gpa, 44Gpa. Gas saturation of these thin sands is approximately 20% uniform saturation from standard RPT.

In order to achieve a robust wedge model, the blocked logs (Figure 4.15) with block size of 5m and Backus averaging was created. The reflectivity was calculated and convolved with the known wavelet, to calculate a synthetic zero offset trace. The reflection coefficient and synthetic traces show the decrease or trough at the top of the sand, while the increase or peak is interpreted as the base of the sand, as marked by the black dashed square in Figure 4.15. By measuring from the top to the base, the thickness of gas sand is 7m from the well log, which is fit well with Gamma ray log.

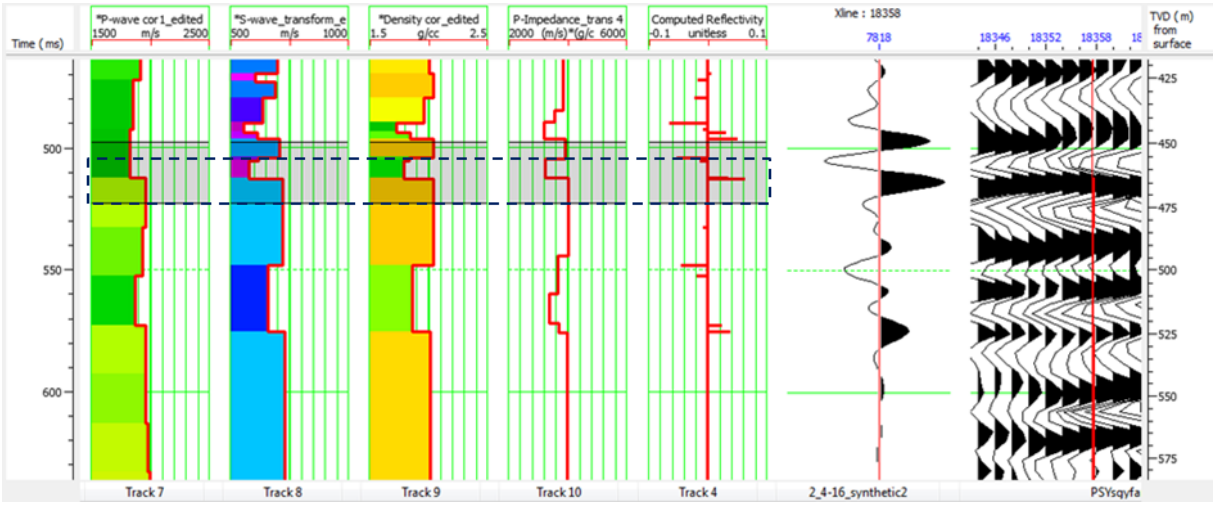

Figure 4.15: Blocked well by backup averaging. Blocked well from left to the right: P wave blocked, S wave blocked, Density blocked, Acoustic impedance blocked, Computed Reflectivity, Synthetic trace, Far stack seismic.

Based on the previous research (Eidissen, K., 2013, [30]), a patchy gas saturation of 70% or a uniform gas saturation of 20% gives the best fit to the data from the presumed

gas-filled area. Then, together with brine saturation, three scenarios will be applied further to build wedge model. We examined the thin bed tuning effect on the AVO response for three cases: 1. a 20% gas uniform saturation bearing wedge; 2. a 70% gas patchy saturation bearing wedge; 3. a 100% water bearing wedge. The densities and P-wave and S-wave velocities of the three different saturation cases were computed in *Hampson-Russell* based on Biot-Gassmann theory.

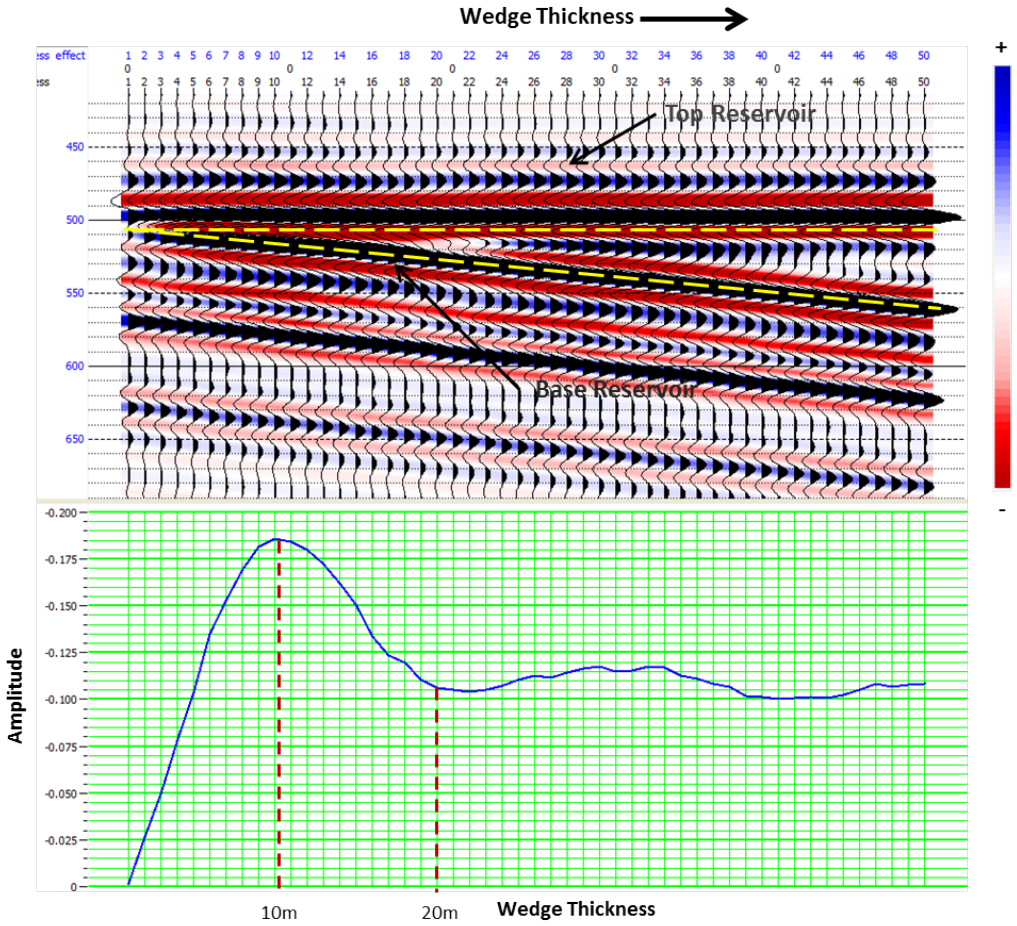

Figure 4.16: Wedge model for 20% gas uniform saturation on the top. Yellow dashed line represents the top and base reservoir respectively. On the bottom: Tuning effect of amplitude versus wedge thickness when picking the top reservoir. Dashed red line marked tuning thickness 10m and threshold thickness 20m.

A synthetic seismogram of the wedge model for the first case (20% gas uniform saturation with far offset wavelet) was shown on the top of Figure 4.16. At the top of the sand, a higher impedance shale to a lower impedance gas sand so reflection coefficient for the top of the sand is negative (a red trough). The numbers at the top of each trace illustrated wedge thickness of the sand at the location of each trace, up to 50m. By

picking the tough horizon, the amplitude tuning curve for Case 1 shows that the tuning thickness is approximately 10m. The threshold thickness of gas sand wedge which is limit of separability shows around 20 m. As the wedge thins to less than 10 m, the magnitude of the amplitude decreases rapidly. Also, the amplitude value between -0.1 and -0.185 could have two corresponding thickness, which could be worth noting to be done further estimation of tuning thickness.

Further curve extraction from *Hampson-Russell* will be demonstrated in the next section. It brings some difficulties to distinguish among those different cases with near and far wavelet by just looking at the curve respectively, so the combination is necessary to be carried out.

Then, this scenario was set as an example demonstrating the tuning effect on AVO response. Each synthetic trace is representative of a corresponding thickness in the wedge model. Thickness changes in this model will represent new pseudo wells (Chapter 3.5.2). Once the well was exported, the gathers of the wedge model could be analyzed in terms of AVO response. The AVO responses were computed from the Aki-Richards equations in *Hampson-Russell*. The AVO responses of the finger horizon below the maximum tuning thickness (2m, 5m), at the maximum tuning thickness (10m), and above the tuning thickness (25m) were shown in Figure 4.17, respectively. From the figure, the difference in AVO response of the tough and peak for different cases can be observed. Each small section of the figure, synthetic seismic section for four different thickness is in upper part, which the horizontal axis represents the offset angle up to 45 degree, vertical axis stands for two way travel time. As the wedge thins to less than 3m, the magnitude of the amplitude decreases rapidly, reaching approximately zero, referring as destructive interference. For example, when thickness approaches 2m, it is hard to distinguish the tough from peak, which brings out almost overlaying AVO response. The AVO response on the trough (red line) at the maximum tuning thickness (10m) is characterized by both a large negative intercept and gradient, whereas that below the maximum tuning thickness (5m) demonstrates a relevant smaller negative intercept and corresponding flat gradient. AVO responses above threshold thickness(25m) displays the similarity with 5m. Based on the survey on tuning effects, it could have the probability of different tuning thickness responding to a similar AVO responses.

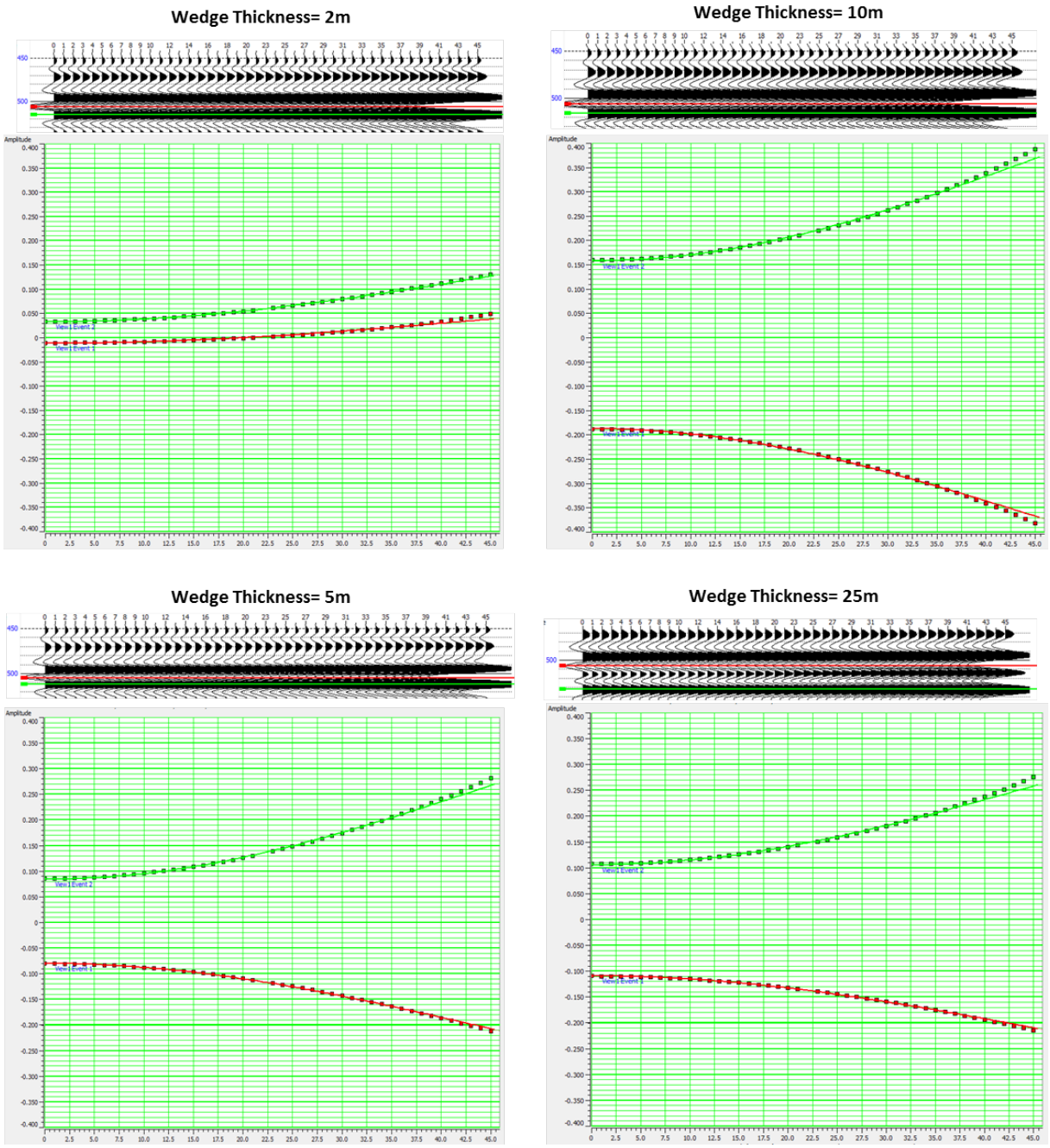

Figure 4.17: Angle gather and AVO response analysis from wedge modelling (Far stack 20% gas uniform saturation). Top left: Tuning within a thin bed (2m), top and base shows overlap behavior. Top right: The maximum tuning thickness (10m) with the largest intercept and gradient; Bottom left: Tuning effect in the middle of maximum tuning effect (5m); Bottom right: Thick sand layer (no tuning effect). Four cases is in the same scale amplitude (-0.4-0.4).

4.7 Normalizing tuning effect curves

Linear regression is a widely used method in the data processing for AVO analysis. Based on two term Shuey's approximation (Eq. 3.5), the amplitude of each trace is plotted against $sin^2\theta$ of its offset and the relationship becomes linear, as seen in the diagram (Figure 3.3). Using linear regression, a line of best fit can now be calculated that describes how the reflection amplitude varies with offset. Offset was transformed into angle, and two terms approximation carried out by *Hampson-Russell*. Since three different scenarios above was conducted for both far and near stack respectively, AVO gradient analysis will be performed on the synthetic seismic to examine specific events within those gathers. It is extremely important to normalize the effects of saturation and offset before the further estimation of tuning thickness. The regression AVO analysis for three different scenarios was shown in Figure 4.18. They had almost the same intercept (-0.225) related to acoustic impedance contrast, but slight differences in intercept due to a small variation in density when conducting shear wave estimation. The yellow line represents brine saturated reservoir, with the characteristic of smaller gradient. The gradient of 20% gas uniform saturation (blue line) illustrated higher than that of 70% gas patchy saturation (red line) where both amplitude clearly decreases dramatically with offset. This large negative gradient results from strong decreases in Possion's ratio when gas filled sand.

According to Table 4.1, the specific angle for both near and far stack is $3 - 14$ degree and $25 - 36$ degree respectively. The average amplitude values were selected for three scenarios in both intervals. The offset range was marked as red dashed lines in Figure 4.18. The relevant values were listed in Table 4.3. Dividing the amplitude value for far stack by the one for near, the scaled factor was calculated to listed on the right column of the table.

Table 4.3: Comparison of amplitude average for different saturation and partial stackings, and calculated scaled factor.

Scenarios	Near Stack	Far Stack	Scaled factor
brine saturated sand	-0.2304	-0.250	1.087
20% gas uniform saturated sand	-0.2354	-0.332	1.479
70% gas patchy saturated sand	-0.236	-0.349	1.412

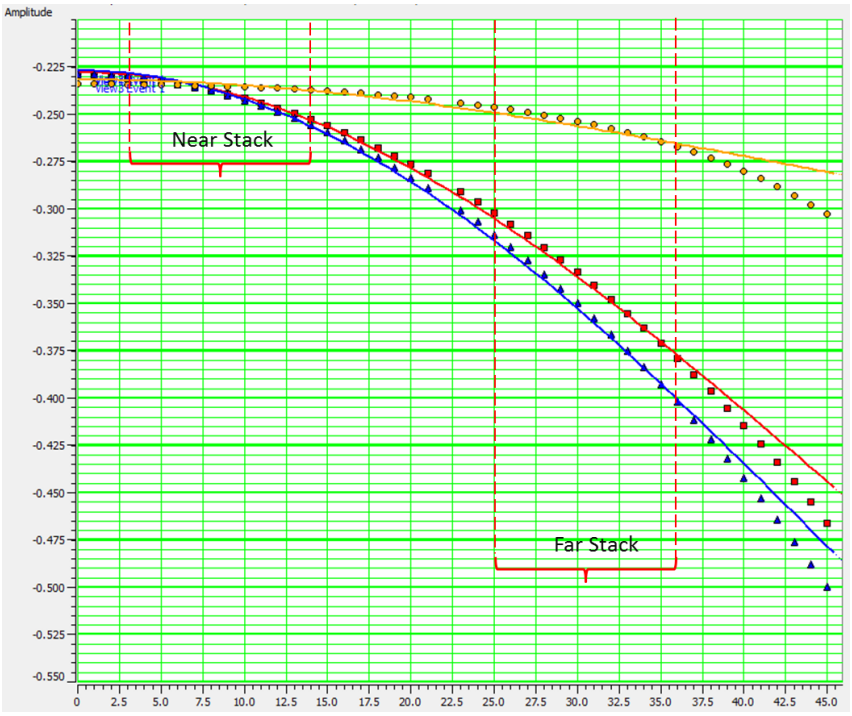

Figure 4.18: AVO gradient analysis for three different saturation scenarios. Yellow line represents brine saturation; red line stands for 70% gas patchy saturation; blue line stands for 20% gas uniform saturation. Horizontal axis represents angle, while vertical axis is amplitude. Red dashed line stands for the range of near and far offset.

Engauge Digitizer was applied to export the tuning curves for each scenario. According to scaled factor, the plot of amplitude versus thickness for far stack can be normalized with near stack. The scaled factor for gas saturation shows much larger differences between different partial offsets than brine saturation. Above the threshold thickness, averaging thickness need to be standardized with corresponding amplitude in Table 4.3. Then normalized near and far stack for brine saturated was shown on the left of the Figure 4.19.Based on the comparison with relative extracted amplitude, the tuning effect curves need to be normalized satisfying two conditions. One is to maintain the relationship between near and far offset, while the other is to set relative amplitude of tuning thickness approaching to 1. The resulting curves are shown on the right of Figure 4.19. Observing slightly higher relative amplitude on near Stack than the one on far stack below tuning thickness, while another side displays the opposite circumstance (between tuning thickness and threshold thickness).

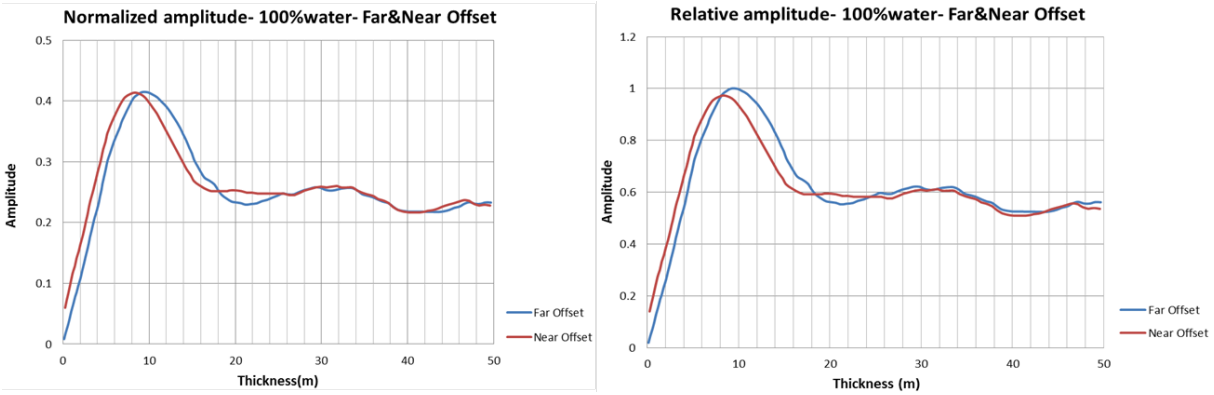

Figure 4.19: Tuning effects amplitude versus thickness for brine saturated reservoir. Left: Normalized amplitude versus thickness; Right: Relative amplitude versus thickness; Red curve represents near offset, while the blue one stands for far offset.

Then the other two scenarios were applied the same approach as brine saturated. The corresponding normalized and relative amplitude versus thickness were shown in Figures 4.20 and 4.21. Compared with the first case, both gas saturated sand exhibited a big difference for near and far stack based on a larger scaled factor. It is interesting to note that the amplitude for below 5m displayed a compactness for both scenarios and then started to display a obvious separation. Near offset close to zero-offset, associating with intercept, while far offset is related to AVO gradient. At the vicinity of the tuning thickness, an apparent higher amplitude gradient was observed than the intercept in tuning curves. When the layer thickness is below tuning, both intercept and gradient amplitude decrease linearly with the thickness decrease.

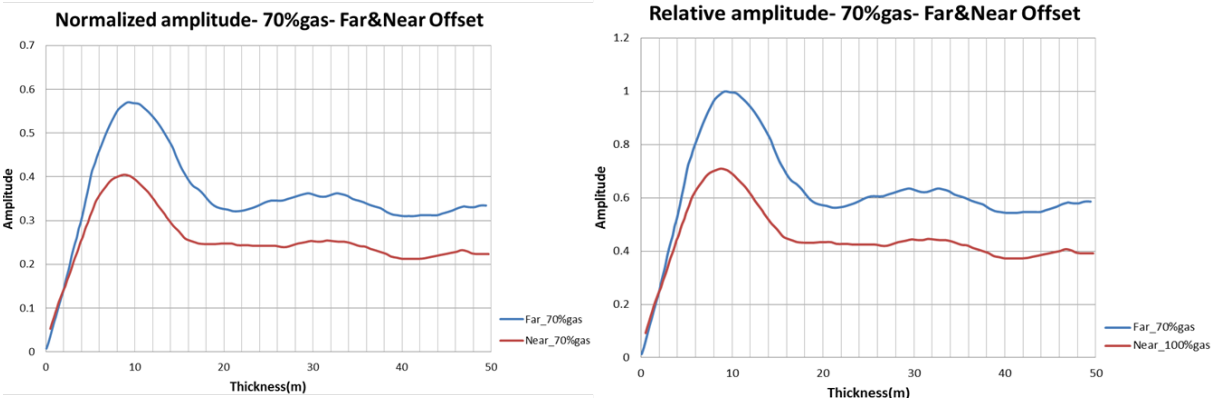

Figure 4.20: Tuning effects amplitude versus thickness for 70% gas patchy saturated reservoir. Left: Normalized amplitude versus thickness; Right: Relative amplitude versus thickness; Red curve represents near offset, while the blue one stands for far offset.

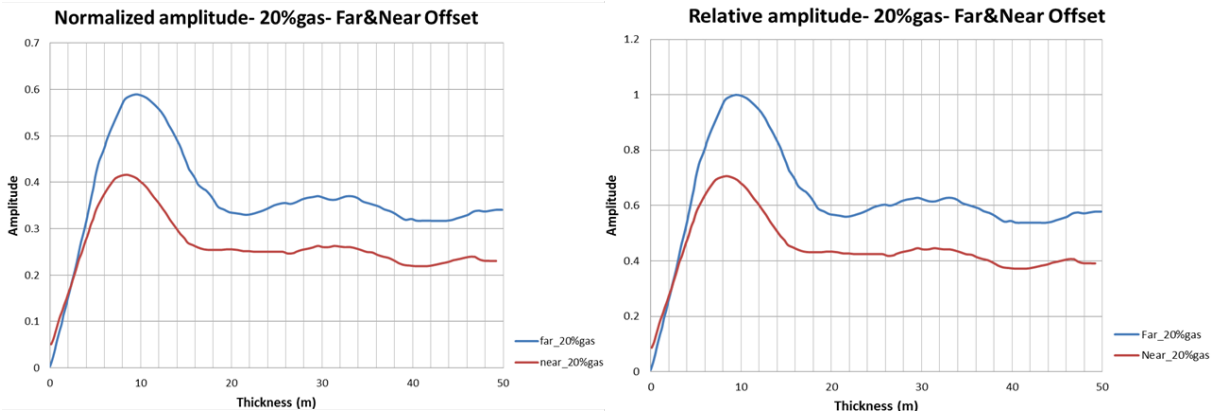

Figure 4.21: Tuning effects amplitude versus thickness for 20% gas uniform saturated reservoir.Left: Normalized amplitude versus thickness; Right: Relative amplitude versus thickness; Red curve represents near offset, while the blue one stands for far offset.

4.8 Inversion model construction

The seismic inversion is excellent at deriving acoustic impedance contrasts across layered interfaces, which reveals short-scale (tens of meters) variations of impedance. More geoscientists understand the concept of impedance and geology than the seismic trace. Thus, working in the impedance domain is a great mechanism for integrating with the various disciplines. Post stack seismic inversion in near offset has been inverted for relative acoustic impedance, and the aim of the inversion was to improve the interpretation of the seismic dataset focusing on target gas sand.

Bandlimited inversion was the first type of post-stack inversion procedure to be performed. The relative P-acoustic inversion using the well 2/4-16 was carried out for the time window 0-1000 ms TWT by inverting near offset seismic data (Figure 4.22). Notice that the acoustic impedance of our target layer as marked the gray arrow is obvious lower than the surrounding layers, as expected in shallow gas zone. This is the starting model for the inversion, where have 'stretched' the impedance based on the structure. Simple acoustic bandlimited impedance inversion is very quick and accessible. The accuracy of acoustic impedance inversion can be increased if the seismic band was expanded to include low frequencies. Model Based Inversion with more geological details will be shown in the Results section.

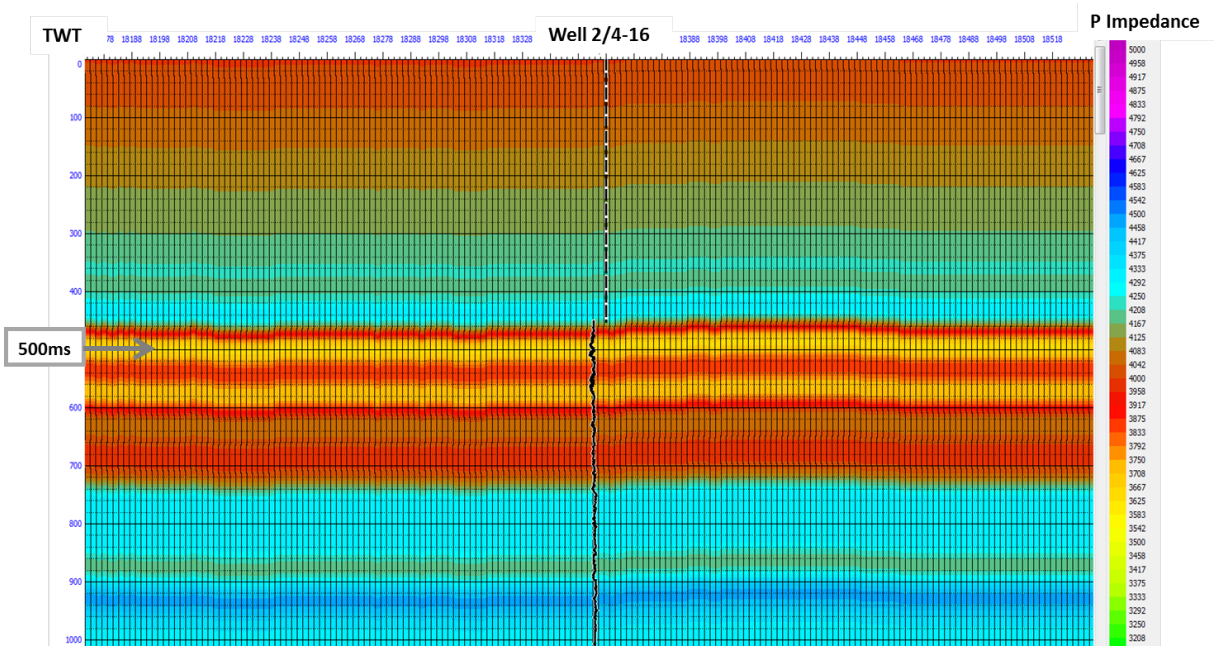

Figure 4.22: Post-stack bandlimited inversion model.The color coding invert P impendance inversion

5 Results

5.1 Sand thickness estimation

Through the modeling processes, an AVO tuning phenomenon has been recognized by observing the differences in amplitude varation between near and far offset trace with respect to the variation between layer thicknesses. A comprehensive comparison for different saturation and offset partial stackings will be shown in Figure 5.1 to bring a better and intuitive overview. Two scenarios were made from partial stacking demonstrates a slightly higher tuning thickness (10m) than the one for near offset (9m). This skewness phenomenon was predominately contributed by major reason offset different moveout and NMO stretching (Lin.L.,and Phair R.,1993, AVO tuning, [31]). The tuning thickness from fat offset is comparable with a quarter of wavelength. The main frequency domain is around 47Hz, while velocity could be estimated as approximately $1900m/s$ from the well log. A rough prediction of tuning thickness can be calculated as:

$$\lambda/4 = 1900/47/4 = 10.1m \tag{5.1}$$

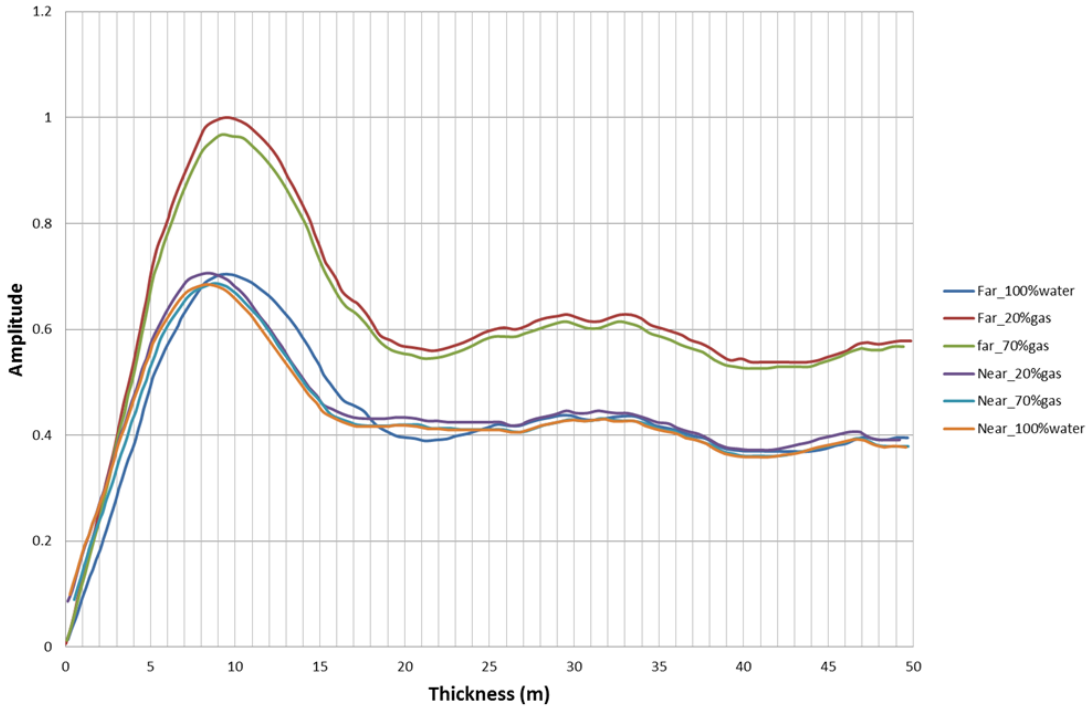

Figure 5.1: Normalized and relative amplitude for different saturation and partial stackings.

A great similarity among those tuning curves for near offset were observed, while two scenarios of gas saturation vary widely with different offsets, but a slightly contrast with 20% uniform and 70% patchy gas contents. It could be predicted that sand thickness is more independent for different gas content in near stack. Besides, we observe the gradient amplitude corresponding to the maximum waveform constructive interference for far stack shows an obvious separation with the one for intercept amplitude (Figure 5.1). This graph could be a great potential tool to distinguish high amplitude anomaly caused by tuning effects from gas saturation.

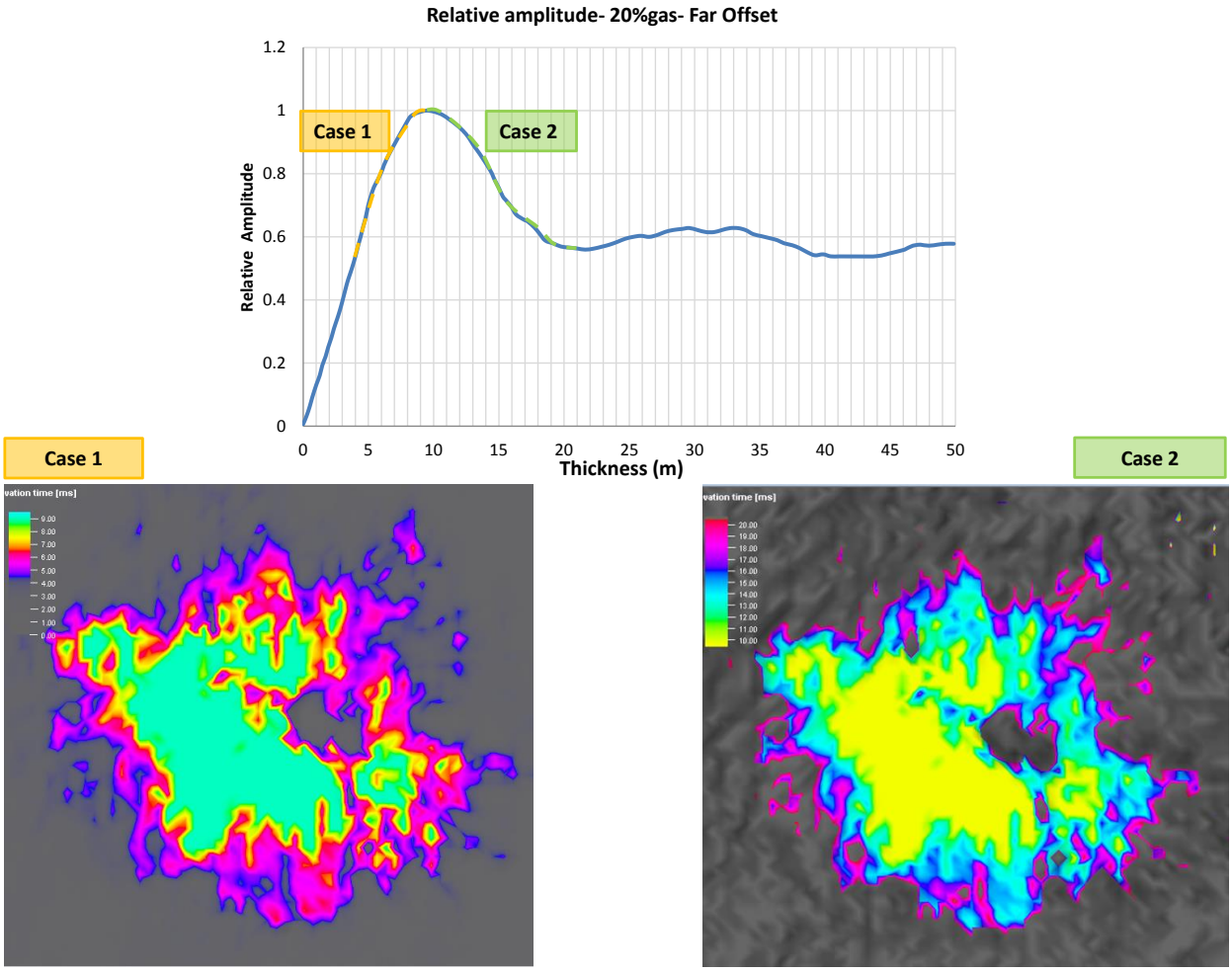

Figure 5.2: Two possibilities of corresponding thickness to the relative amplitude. The estimated thickness map for both cases in the bottom (20% uniform gas saturated as an example).

Tuning thickness is a function of the bandwidth of the wavelet in the seismic data and not of the relative reflection coefficient strengths for the top and base of the sand.

This means that once we have determined what the tuning thickness is and have identified the tuning amplitude we can calibrate the amplitude information in the seismic data and measure the thickness of a thin sand. At the vicinity of tuning thickness, the apparent high amplitude could be raised by two possibilities of thickness. The relationship could be considered as linear, while polynomial regression type was applied to achieve more accurate relationship between relative amplitude and sand thickness. As shown in Figure 5.2, two thickness maps were calculated respectively for two cases. Geologically, the map shows low possibilities to exist a thin sand between tuning thickness and onset thickness (Case 2). Then corresponding sand thickness estimation will be carried out focusing on the pinching out zones below the tuning thickness.

As depicted in Figure 5.1, the relationship could be considered as linear for thin layer in the pinching-out zones, avoiding the areas where the top and base of sands are resolved as separate reflectors in the seismic data. The well-log show evidence of around 7m thickness sand, where sands are expected to be thinner than tuning thickness. The calculated thickness maps of near and far stack for different gas scenarios are shown in Figures 5.3 and 5.4.

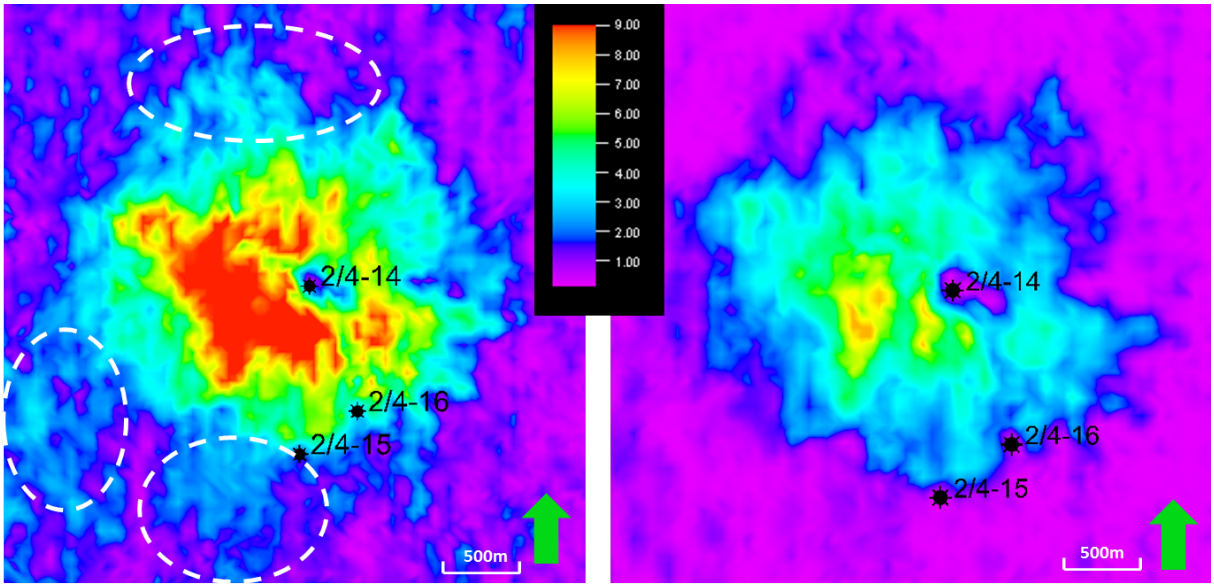

Figure 5.3: Thickness map of 20% uniform gas for both far and near offset. The color legend is sand thickness, which set to be equal (0-9m).

The color legend represents sand thickness. Thickness map of 20% uniform gas for both far and near offset demonstrates a big difference above 5m, which corresponds to the green color. The horizontal extent was evaluated as approximately 1.85Km. The

fingering pattern is observed in both near and far offsets. Besides, the migrating pattern marked as the white circles is obvious to be distinguished from far stack in contrast to near stack. A similar trend observed in both the tuning thickness curves for 20% uniform gas and 70% patchy gas saturation, signifies the analogical estimation of sand thickness due to the linear relationship.

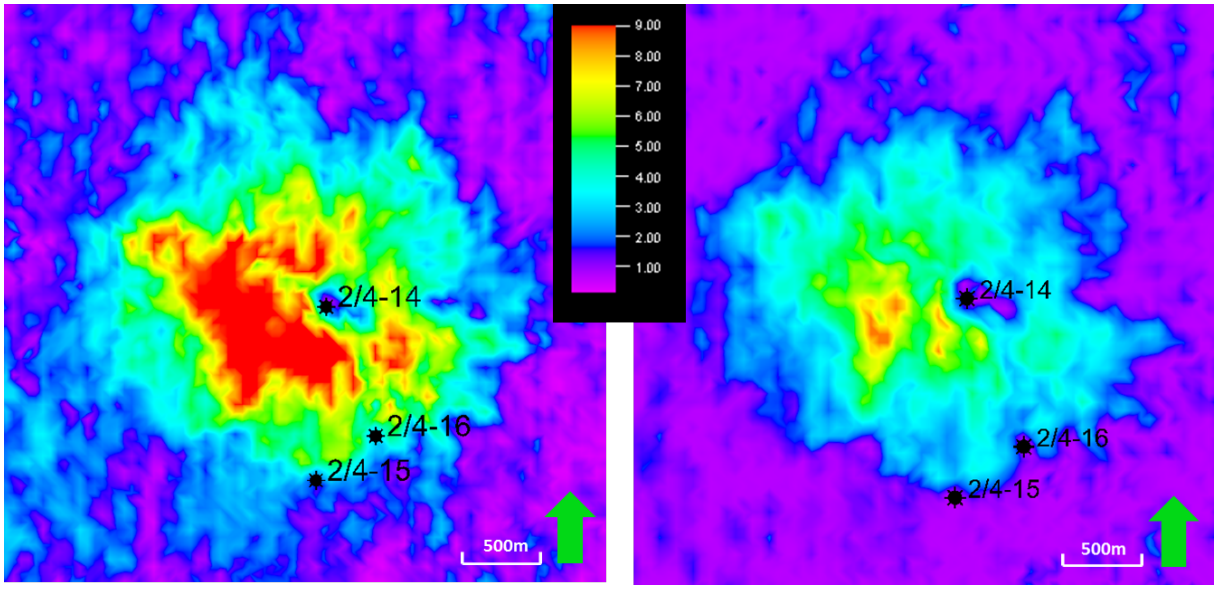

Figure 5.4: Thickness map of 70% uniform gas for both far and near offset. The color legend was set to be equal(0-9m).

5.2 Inversion model

Seismic inversion for acoustic impedance is a well-established tool where it has become a widely used method for optimizing the quantitative analysis of seismic data. Recently, the focus has been widened to also include the shallow subsurface as this may be of interest to more detailed studies of geological processes.

Model based inversion was constructed on the foundation of initial model band-limited inversion (Figure. 5.5). By analyzing the errors or "misfit" between synthetic and real trace, each of the layers is modified in thickness and amplitude to reduce the error. This is repeated through a series of iterations. By changing the value of iteration, we approach less error between synthetic from well and real trace. Although, the model still has limitations, the model based inversion looks more detailed and geologically reasonable compared with band-limited inversion model.

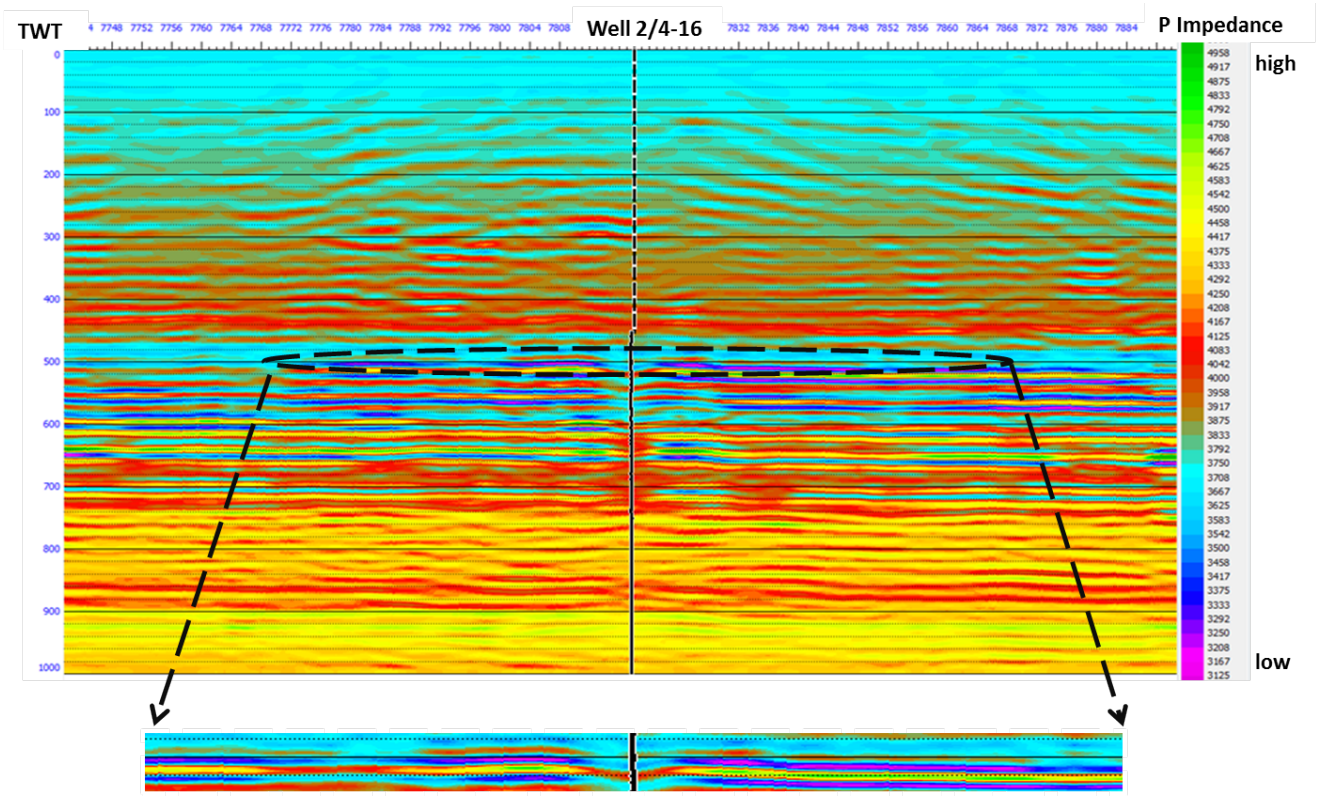

Figure 5.5: Model based inversion model. The color coding invert P impedance. Highlighting target horizon is zoomed on the bottom.

With seismic inversion model, we are able to analyse layers or lithological units. The result from the inversion is an acoustic impedance volume. Black circle is marked as a close view of our target horizon, with the expected character of low acoustic impedance in gas sand. The acoustic impedance geologically increases with the depth. Many thin gas sand layers with low acoustic impedance were also discovered in shallow depths (approximately at 550ms, 560ms and 600ms). In areas with good well control, this methodology allows us to successfully integrate the extent of seismic high amplitude anomaly and low acoustic impedance.

Vertical resolution is improved as seismic inversion attempts to remove the effects of the wavelet. This benefit gained from the inversion of broadband data will help to better define the extent of high amplitude anomaly and decrease the uncertainty in tuning effects. Figure 5.6 is a vertical time slice through acoustic impedance volume showing the fingering shape horizon, it displayed relevant lower impedance in the central blowout area (shown in blue Figure 5.6). Some grids displayed in the acoustic impedance map due to the limit uploading operation of horizon surface map, it can be ignored since it does

not affect the blowout area. The close window displayed a channel shape pattern marked as a circle. The difficulties of interpreting this pattern depends on the reliability of the inversion model, seismic data quality and the direction of seismic survey. It was evaluated that the horizontal extent with low acoustic impedance is approximately 1.9Km. The distance range of low P-impedance is more comparable with the area of wide variation between different offset partial stackings (Figure 5.3). No apparent fingering shape pattern is displayed compared with RMS amplitude extraction in blowout area. It could be a powerful evidence that high amplitude anomaly not only affected by gas saturation, but also by tuning effect.

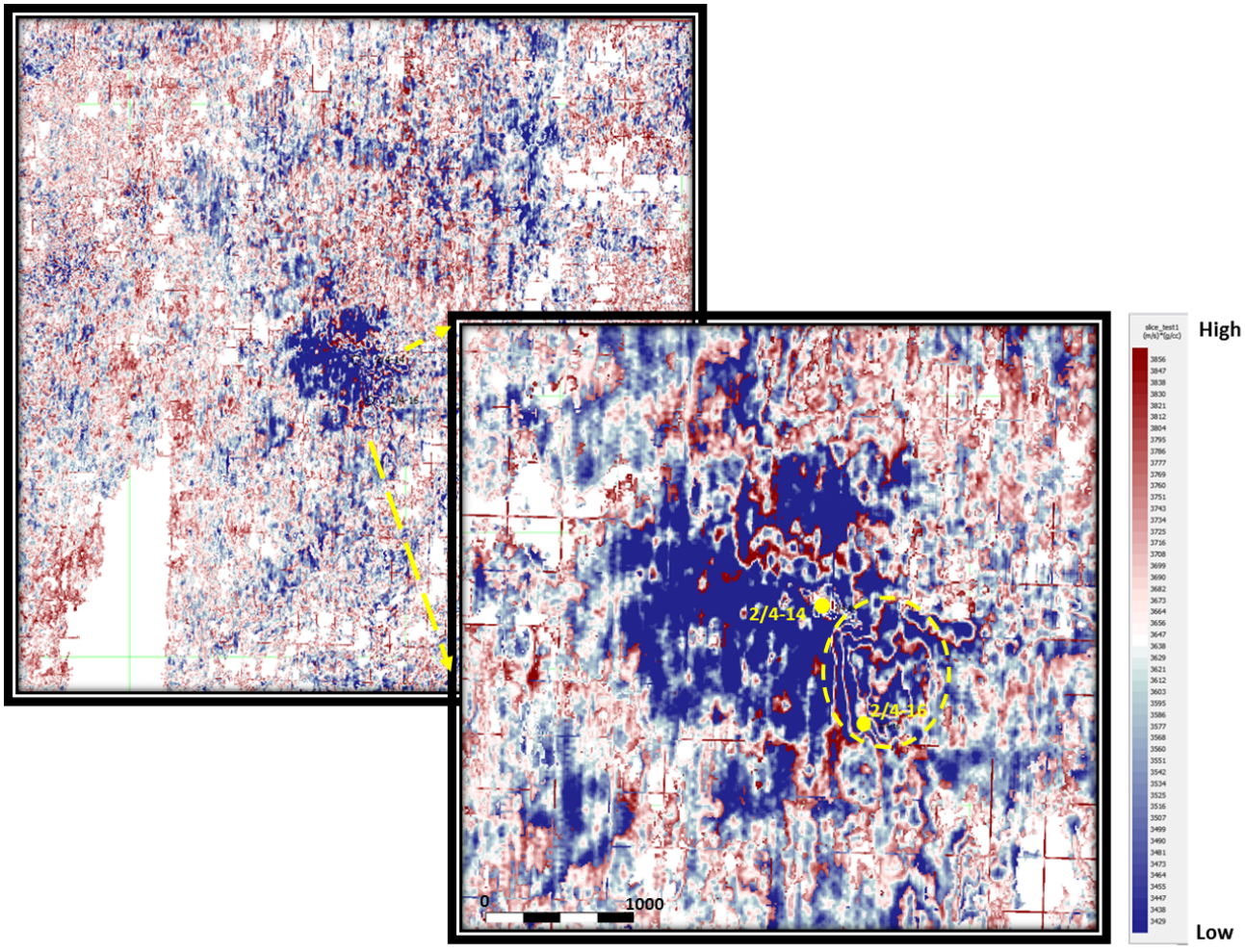

Figure 5.6: Time slice around 520ms from model based inversion model. Blue color represents low acoustic impedance; Yellow circle illustrates a channel shape pattern.

6 Discussion

The work done in the master's thesis has been focused on performing AVO attribute analysis and sand thickness estimation by tuning effect analysis. Some uncertainties of constructing wedge model will be discussed in this section first. In the next section, how to distinguish between gas saturation and tuning effects of observed high amplitude anomaly will be discussed according to the analogical partial stacking results.

6.1 Uncertainties on wedge model construction

Two seismic data sets- near and far stack associated with one of the wells were used in the thesis. Properly balanced seismic data is the first crucial step for further analysis. When we calculated the scaled factor between them, several attempts were conducted, no exactly the same values could be expected. This signifies that it is uncertain certain about scaled factor obtained accurately by simply balancing the data sets.

Wavelet extraction is a vital factor for creating the synthetic seismic gather and wedge model. It was chosen to use the extracted wavelet from seismic instead of well since lack of available check shot and poor well tie coefficient. Since our target area is quite shallow, a refined wavelet extraction is necessary. Some uncertainties and inaccuracy exist when avoiding low frequency effects. The well tie is often centered on the interesting part of the well, and then shifted on the synthetic seismic (above 1000ms). There is also the possibility that the shifting of the reflectors is a result of some wrong measurements performed in the well.

When constructing the wedge model, blocked well log, as an initial upscaling procedure, was applied to achieve a better wedge model by analyzing the tuning thickness. Blocking well logs has no unique solution, with three available different functions in *Hampson-Russell*. In the end, backus average brings a more reasonable model compared with the other two modes: automatic uniform and automatic non-uniform. In order to build robust synthetic seismic traces which tough-peak matching accurately with acoustic impedance boundary, backup average 5m blocking size was applied in the end. It was uncertain that it could be an optimal blocking mode for wedge application since synthetic seismogram computed differences between the fine scale log and raw log was not conducted in this thesis. Blocking size can also bring unstable estimation.

The absence of recorded shear-wave data imposes severe limitations in sand evaluation and wedge model construction. The accuracy of the shear-wave velocity estimation is important especially when performing AVO modeling. It leads to some uncertainties to conduct our estimation of shear wave. P-wave velocity depends highly on how the gas is saturated in the pore space such as uniform or patchy, the amounts of gas estimated from the P-wave velocity contains high uncertainty. For this thesis, 20% uniform gas saturation and 70% patchy gas saturation were applied to achieve rock properties prediction in the reservoir based on the previous research. It is not straightforward to implement our saturation distribution was decided by 600ms AVO analysis, since RMS amplitude extraction from our target area demonstrated an obvious gas anomaly compared with 600ms. Therefore, it is clear that different gas distribution brings out uncertainties. Besides, patchy saturation and uniform saturation are considered to be extreme cases of saturation distributions, while leads to some differences within the reality conditions in the reservoir.

Another uncertainty stems from Gassmann's assumption that the rock is monomineralic. The amount of shale in the shallow area can be a subject to mention affecting the rock properties prediction.

6.2 Discriminating thickness changes from saturation and tuning effects

In relative soft sands, the impact of increasing porosity and hydrocarbon saturation tends to increase the seismic amplitude, and therefore works in the same "direction" to layer thickness (Avseth et al.,2005, [17]). It brings some difficulties to discriminate layer thickness changes from gas saturation and tuning effects. The bright trough/peak seismic amplitude on stacked data is acknowledged to be associated with plenty of gas-filled sand within the shallow depth. By analyzing the relationship of amplitude and tuning thickness between the near and far stack, a feasible approach for implementing the discrimination of saturation and tuning effects will be discussed in this section.

Figure 6.1 left side shows the corresponding thickness map and relative amplitude extraction map for near stack. The right bottom diagram illustrates that saturation is not a critical factor for near stack since relative amplitude as a function of layer thickness is not mainly affected by gas saturation. Therefore, it could be deduced that high amplitude

is mainly related to thickness variation for near stack. It is also interesting to note the fingering shape pattern is displayed obviously in the thickness map. It will represent the most likely high amplitude associated with tuning effects rather than gas saturation. The most likely possibility of this circumstance is shown in the sketch on the right top. Visualization of the output demonstrated pinching out pattern from the blowout well. The maximum likelihood tuning effects is associated with destructive interference below limit thickness of visibility, while constructive interference occurs when layer thickness is between a half and a quarter of a wavelength, corresponding to the range of 4m and 9m. The color legend of sketch is relevant to the thickness map. The destructive and constructive interference can be successive observed from blowout well.

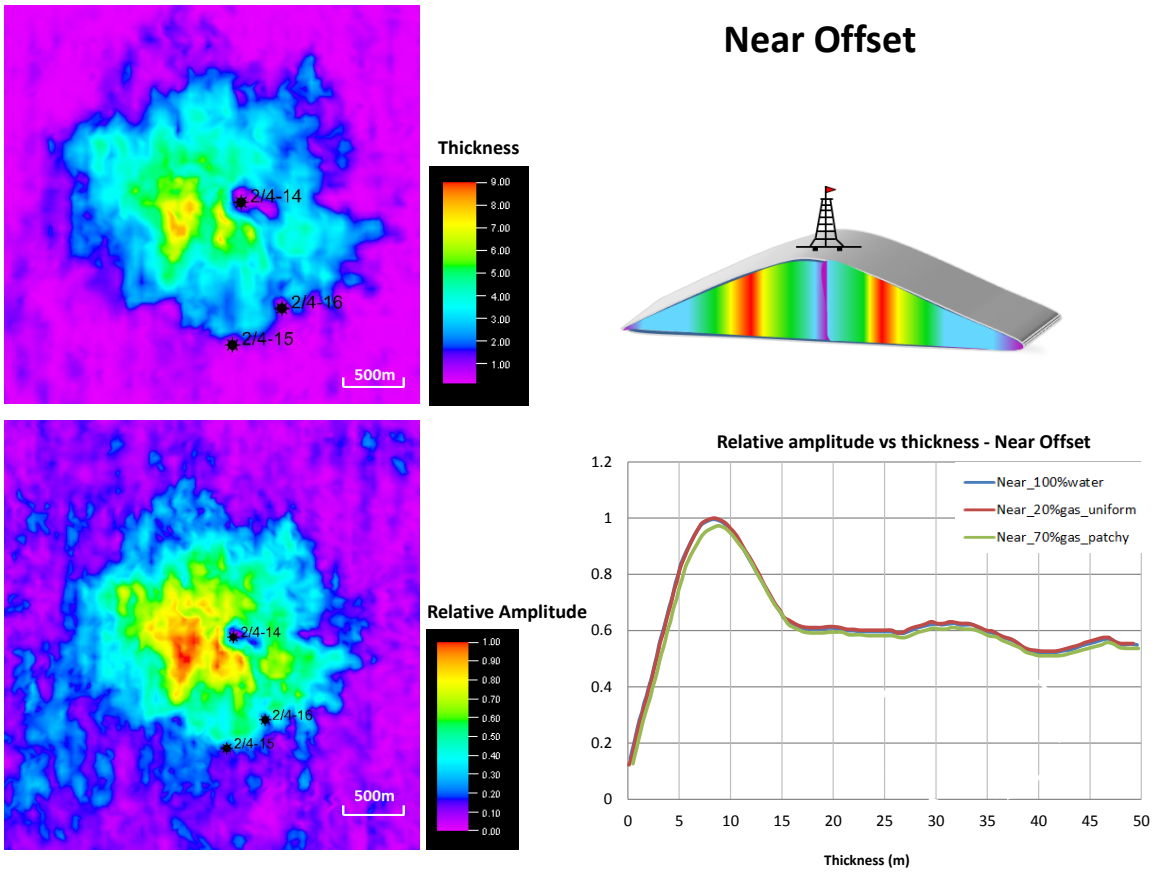

Figure 6.1: Combination of the near stack effects. Top left: Thickness map; Bottom left: Relative amplitude map; Top right: A possible sketch of tuning effect; Bottom: A diagram of tuning effect curves both Near and Far Offset.

The same visualization exhibition was arranged for far stack. In Figure 6.2, we explore how thickness variability might be associated with gas filled or tuning effects. The

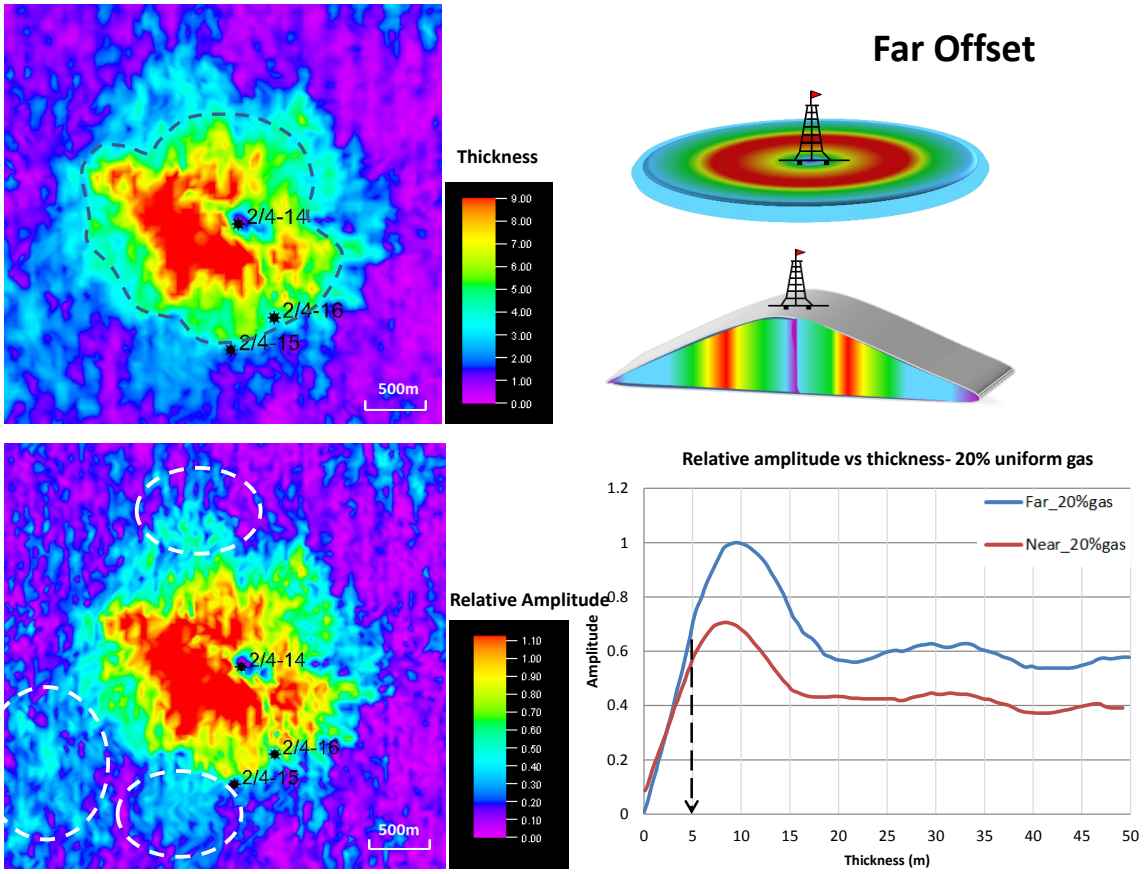

Figure 6.2: Combination of the far stack effects. Top left:Thickness map; Bottom left: Relative amplitude map; Top right: A possible sketch of tuning and gas saturation effect; Bottom: A diagram of tuning effect curves both Near and Far Offset.

combination of thickness map and relative amplitude as a function of thickness diagram, allows us to distinguish two inducing factors for high amplitude, would greatly improve our interpretation. The thickness map demonstrates a different distribution combined with near stack above 5m, which corresponding to the green color, as marked by the dashed line. The obvious separation of different offsets could be discovered in right bottom diagram around 5m, where gas saturation starts to affect the amplitude significantly. Inside marked reservoir with the calculation of approximately $2.92km^2$ is most likely related to plenty of high pressure, where gas saturation plays a dominant role. By contrast, a most likely statement of arising bright amplitude could be due to tuning effect outside the marked area. There are some indications that green color could be barely discovered in the fingering shape pattern. It supposed that tuning effect could be a dominant factor compared with gas content. Besides, some interesting sections marked as white circles

indicate tuning thickness around 4m. The possible explanation for gas migration pattern is less influential, which more relys on tuning effects.

Other two complement tools AVO cross-plot and seismic inversion model have been performed to help classifying and improving the interpretation of high amplitude anomaly. The cross plotting result would be influenced by the assumptions of gradient and intercept from the near and far stack. The roughly estimated extent of gas anomaly from cross-plot is relatively small compared with high amplitude blowout event from RMS extraction. Besides, in the seismic inversion model, the distance range of low P-impedance is more comparable with the area marked in Figure 6.2. These phenomena could be supposedly attributed to tuning constructive amplitude effects.

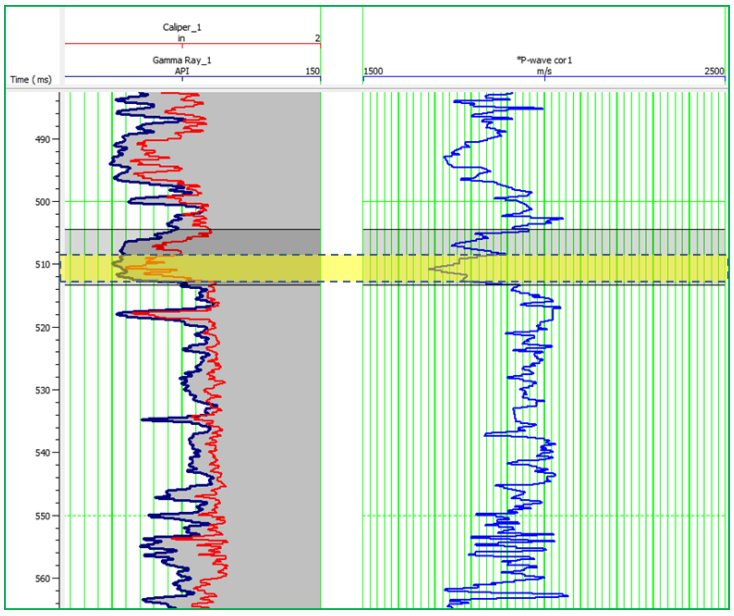

Figure 6.3: Well caliper with Gamma Ray and P-wave velocity displayed a possible thinner sand.

The calculated thickness map in Figure 6.2 indicated approximately a 3m sand around well 2/4-16, which is much thinner than 7m from well data. A close view of well log with caliper and P wave velocity was shown in Figure 6.3. Caliper log curve shows a bad borehole quality which brings some uncertainty to measured log curves as sonic log. Combined with velocity log, most likely explanation of sand thickness is 3m. Geologically, this blowout area can be more likely interpreted that thickers out in the middle (around 7m) and generally decrease in thickness from the center to the edges (pinched out to 3m).

7 Conclusions

The tuning effect, as one of the most serious factors hampering confident lithology and fluid interpretation from seismic data, must be considered, especially for thin-bed interpretation. Thin bed response is one of the key concerns in seismic amplitude interpretation, owing to tuning effect that depends on both thickness and offset.

This study quantifies the AVO tuning effect and sand thickness estimation from seismic amplitude. The seismic tuning analysis results suggest that not only is the observed high amplitude anomaly affected by gas saturation, but also by tuning effect. Near offset close to zero-offset, associating with intercept, is an important indicator for determining the lithology and porosity. High amplitude increase in near offset is more related to tuning effect rather than gas content. Yet, far offset is more related to AVO gradient, which is more effective for differentiating the hydrocarbon sand from the brine sand. The chance of high amplitude anomaly in far offset can be associated with both gas content and interference effects. Therefore, near offset is more reliable to estimate the sand thickness since far offset can be difficult to discriminate layer thickness changes from lithology and fluid changes.

The seismic inversion results indicate that the extent of low P-impedance in gas blowout area is comparable with high gas content of thickness map in far offset. The estimated extent of low acoustic impedance is associated with gas filled sand area rather than interference effects. It could be another evidence that fingering shape pattern can more likely attribute to tuning effects. This poststack inversion model improves the interpretation, which is encouraging to be a complement tool with traditional AVO modelling.

Combined tuning analysis with seismic inversion model conducted in this thesis, the high amplitude anomaly in the blowout area is most likely interpreted that it is thinner on the edges (pinched out) and thick in the middle and generally increasing in thickness from the edges to the center. The fingering shape pattern is more likely due to tuning effects. As a result, the tuning due to the layer thinning creates a dramatic effect on the amplitude gradient since the amplitude gradient is constructively enhanced by the impedance contrast and Vp/Vs ratio. Therefore, the geoscientists should be fully aware of the tuning effect when AVO is used to explore the global sedimentary basins.

References

[1] Haavik, K., Landrø, .M.,2013, Ice Scours as Trapping Mechanism for Shallow Gas. Extended Abstract 75th EAGE Conference & Expedition.

[2] NORLEX, Nordland formation, Retrieved from: http://nhm2.uio.no/norges/litho/nordland.php

[3] Charles, T.F., Ian,A.K., Lawrence, J.P., 1990, Ekofisk Field–Norway Central Graben, North Sea. Field studies

[4] NPD Fact pages. Well 2/4 − 14, Retrieved from http://www.npd.no/engelsk/cwi/pbl/en/well/all/1343.htm

[5] Landrø, M., 2011, Seismic monitoring of an old underground blowout - 20 years later. First Break, 29(June), 39-48.

[6] Ostrander, W.J., 1984. Plane-wave reflection coefficients for gas sands at nonnormal angles of incidence. Geophysics 49 (10), 1637-1648.

[7] Shuey, R. T., 1985, A simplification of the Zoeppritz equations: Geophysics, 5O, 609-614.

[8] Zoeppritz, K., 1919, Erdbebenwellen VIIIB, On the reflection and propagation of seismic waves: Göttinger Nachrichten, I, 66-84.

[9] Rutherford, S.R. and Williams, R.H., 1989, Amplitude-versus-offset variations in gas sands: Geophysics, 54, 680-688.

[10] Aki, K.T., and Richards, P.G., 1980, Quantitative Seismology: Theory and Methods: Vol. 1, W.H. Freeman and Co.

[11] Koefoed, O., 1955, On the effect of Poisson's ratios of rock strata on the reflection coefficients of plane waves: Geophysics Prospect, 3, 381-387.

[12] Smith, G.C. and Gidlow, P.M., 1987, Weighted stacking for rock property estimation and detection of gas: Geophys. Prosp., 35, 993-1014.

[13] Ross, C.P., and Kinman, D.L., 1995, Non-bright spot AVO: Two examples. Geophysics, v. 60, p. 1398-1408.

[14] Castagna, J.P. and Swan, H.W., 1997, Principles of AVO crossplotting: The Leading Edge, 16, 337- 342.

[15] Castagna, J. P., and Swan, H.W., and Foster, D. J., 1998, Framework for AVO gradient and intercept interpretation, Geophysics, Society of Exploration Geophysicists, 63, 948–956.

[16] Avseth, P., Anders Dræge, Aart-Jan van Wijngaarden, Tor Arne Johansen, and Arild Jørstad. Shale rock physics and implications for AVO analysis: A North Sea demonstration: The Leading Edge, June 2008: 788-797

[17] Avseth, P., Mukerji, T. Mavko, G., 2005, Quantitative Seismic Interpretation: Applying Rock Physics Tools to Reduce Interpretation Risk, Cambridge University Press, Cambridge, UK.

[18] Dvorkin, J. and Nur, A., 1996, Elasticity of high porosity sandstones: Theory of two North Sea data sets, Geophysics, 61, 1363-1370

[19] Voigt, W., 1910, Lehrbuch der Kristallphysik. Leipzig : Teubner.

[20] Reuss, A., 1929, Berechnung der Fliessgrenzen von Mischkristallen. Z, Angew. Math. Mech, v. 9, p. 49-58.

[21] Gassmann, F., 1951, Über die elastizität poröser medien: Vierteljahrss-chrift der Naturforschenden Gesellschaft in Zurich, 96, 1-23. The English translation of this paper is available at http://sepwww.stanford.edu/sep/berryman/PS/gassmann.pdf.

[22] Mavko, G., T. Mukerji, and N. Godfrey, 1995, Predicting stress-induced velocity anisotropy in rocks: Geophysics, 60, 1081.

[23] Ødegaard, E, and Avseth, P., 2003, Interpretation of elastic inversion results using rock physics templates, EAGE Ann. Mtg Extended Abstract.

[24] Mindlin, R., 1949, Compliance of elastic bodies in contact, Journal of Applied Mechanics, 16, pp. 259-268.

[25] Hashin, Z. and Shtrikman, S., 1963, A variational approach to the elastic behavior of multiphase minerals. Journal of the Mechanics and Physics of Solids, 11, pp. 127-140.

[26] Chung, H., Lawton.D.C, 1999, A quantitative study of the effects of tuning on AVO effects for thin beds, Canadian Journal of Exploration Geophysics, 35, 36,42

[27] Widess,M.B., 1973, How thin is a thin bed? Geophysics, 38, 1176-1180.

[28] Charles, P., and John, C., 2008, Layer-thickness determination and stratigraphic interpretation using spectral inversion: Theory and application.Society of Exploration Geophysicists, v. 73 no. 2 p. R37-R48.

[29] Yong, X., and Satinger, C., 2007, Improving AVO fidelity by NMO stretching and offset-dependent tuning corrections, The leading EDGE.

[30] Eidissen, K. 2013, AVO-analysis of potentially gas filled shallow gas sand layer. Unpublished Project Report, Norwegian University of Science and Technology (NTNU).

[31] Lin,L., and Phair,R.,1993, AVO tuning. Soc. Expl.Geophys.63rd Ann.Mtg, Expanded Abstracts, 727-730.

A Appendix

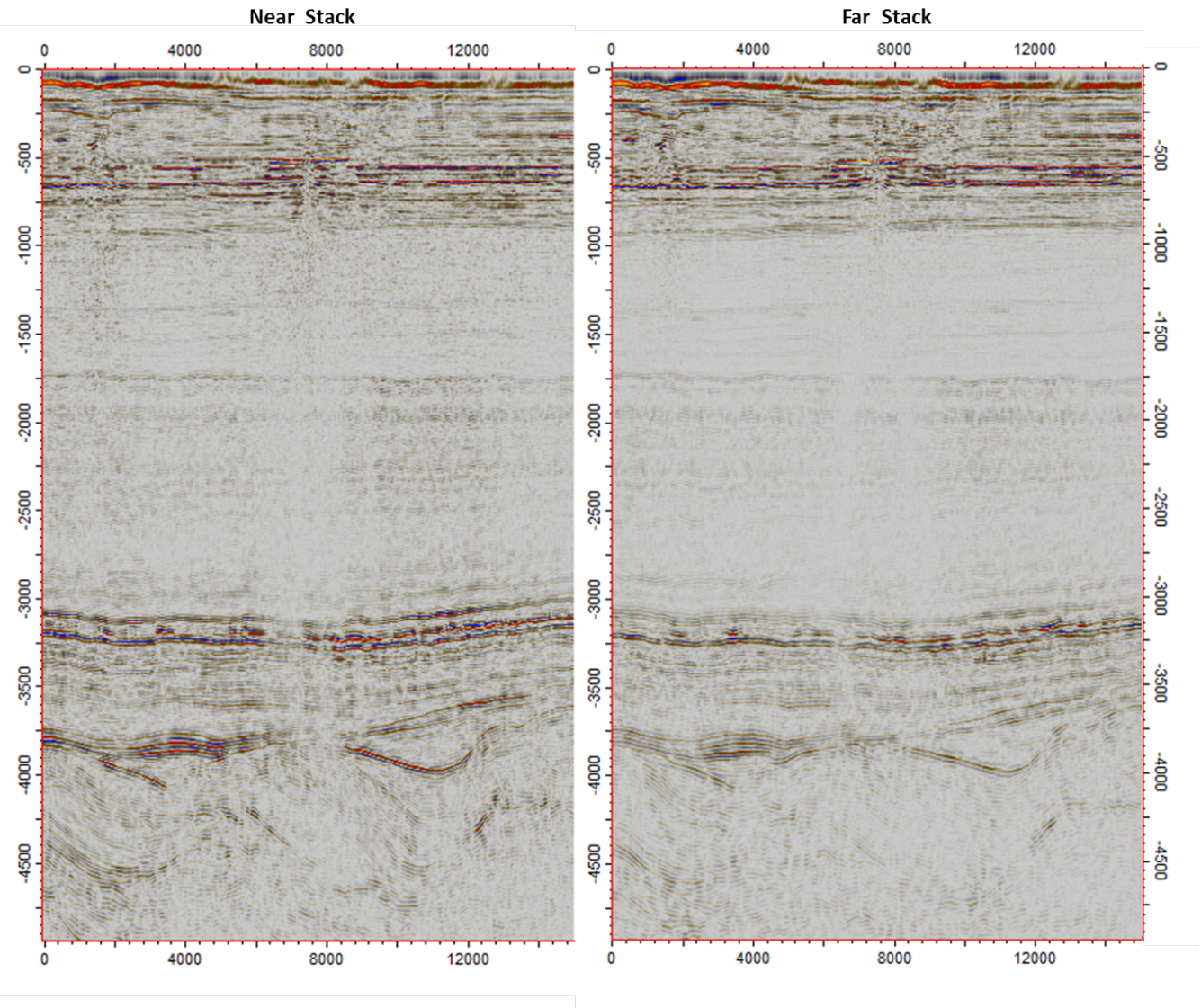

Figure A.1: Original near and far stack seismic data is not well balanced.

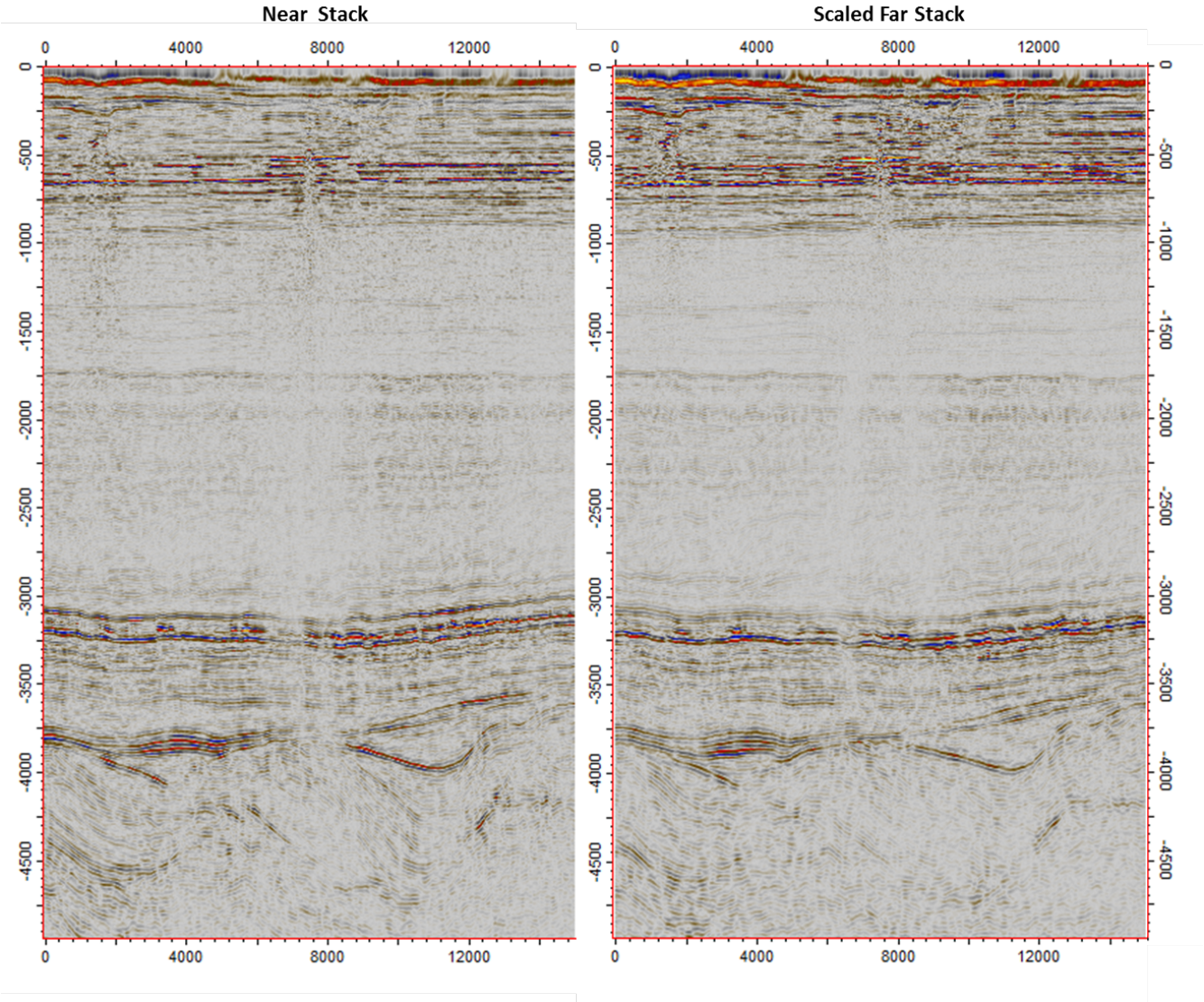

Figure A.2: Near and scaled far stack seismic data is well balanced.

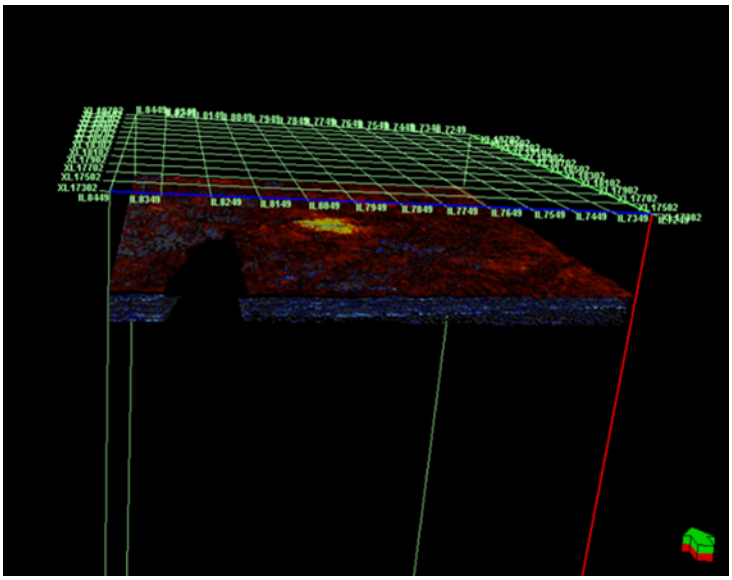

Figure A.3: The procedure of geoboday interpretation is to extract the target gas anomaly.

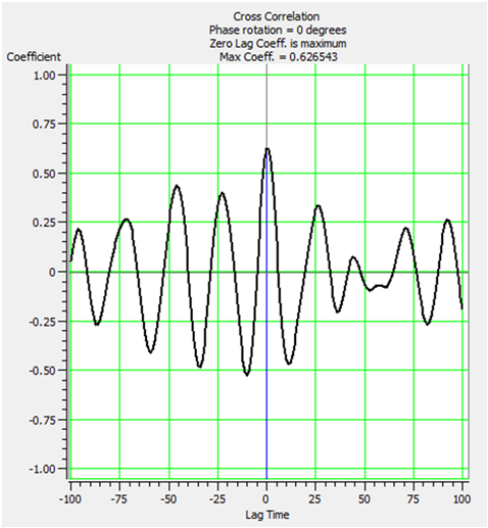

Figure A.4: The well coefficient window.